Chapter 3

Steady State Model Development and Validation

In this Chapter the development and validation of steady state models of various comminution unit operations and the Northparkes Mines grinding circuit are described. Discussion of the steady state models is required as they are the foundation of the developments detailed in Chapters 4 through 7, especially the models of the SAG mill, oversize crusher, primary cyclones and SAG mill discharge screen. The source of the data utilised for model validation is detailed in Section 3.2. The development and validation of the unit operation models in isolation is described in Section 3.3. The linking of the unit operation models to form the Northparkes Mines grinding circuit and the circuit model validation are described in Section 3.4. Further model validation, against published data (Gault, 1975), is presented in Section 3.5.

The foundation of the modelling work in this Chapter and those that follow is that of the Julius Kruttschnitt Mineral Research Centre, which has studied and modelled autogenous (AG) and semi-autogenous grinding (SAG) mills for over twenty (20) years (Morrell and Delboni Jnr, 1996). Their "Variable Rates" AG/SAG model (utilised in this work) is "arguably ... the only one that is widely used ... for design, pilot mill scale-up and optimisation" (Morrell et al., 2001), which reflects the quality and depth of their research programme. These models are gaining wider acceptance and are being utilised for mill scale-up, design and optimisation (Morrell, 2004).

3.1 Model Development Logic

This Section provides an overview of logic behind the development and utilisation of the models presented in Chapters 3, 4 and 5.

In Chapter 3, the steady state models of the unit operations that make up the grinding circuit at Northparkes Mines are described. The basis of the steady state models is the extensive modelling work conducted by the Julius Kruttschnitt Mineral Research Centre.

The models are realised in the MATLAB-Simulink environment in the model development sections. This development serves two purposes. Firstly, replicating the results of commercially-available software demonstrates that the models have been correctly coded in the MATLAB-Simulink environment. Secondly, sufficient confidence in the steady state model coding allowed the progression of the research towards the final goal of the development of inferential measurement models.

The physics behind the steady-state models is not described in detail in this Thesis. Such description is beyond the scope of this research. Furthermore, the model physics is described in detail elsewhere (Whiten, 1974), (Lynch, 1977), (JKTech, 1994), (Morrell and Delboni Jnr, 1996), (Napier-Munn et al., 1996), (Valery Jnr., 1998), *etc.*

Dynamic models of the SAG mill ball charge, rock charge, water charge and mill liner weight are presented in Chapter 4. The SAG mill ball charge and mill liner models are novel to this research and the associated physics and logic are presented alongside the development of the model equations.

The SAG mill rock and water charge models are dynamic extensions of the steady state models presented in Chapter 3 and draw heavily from the work of Valery, (Valery Jnr and Morrell, 1995) and (Valery Jnr., 1998), who was conducting research at the Julius Kruttschnitt Mineral Research Centre at that time.

The presentation and development of dynamic models was required for their utilisation in the Combined State and Parameter Estimation model formulations presented in Chapter 7 and described in one of the the journal papers resulting from this research: Apelt et al. (2002a).

Chapter 5 describes the inferential measurement models of the SAG mill inventories, fresh feedrate and discharge rate and the corresponding size estimates. The development of these inferential models was a key objective of this research. The inferential models have been described in two further journal papers resulting from this research: Apelt et al. (2001a) and Apelt et al. (2002b).

The models are subjected to model validation, sensitivity analysis (also detailed in these two journal papers) and case-study type applications in Chapters 5, 6 and 8, respectively. The model demonstration on plant data, construction of a SAG mill operating curve and MVC development and simulation constitute the content of the next journal installment (Apelt and Thornhill, In Press).
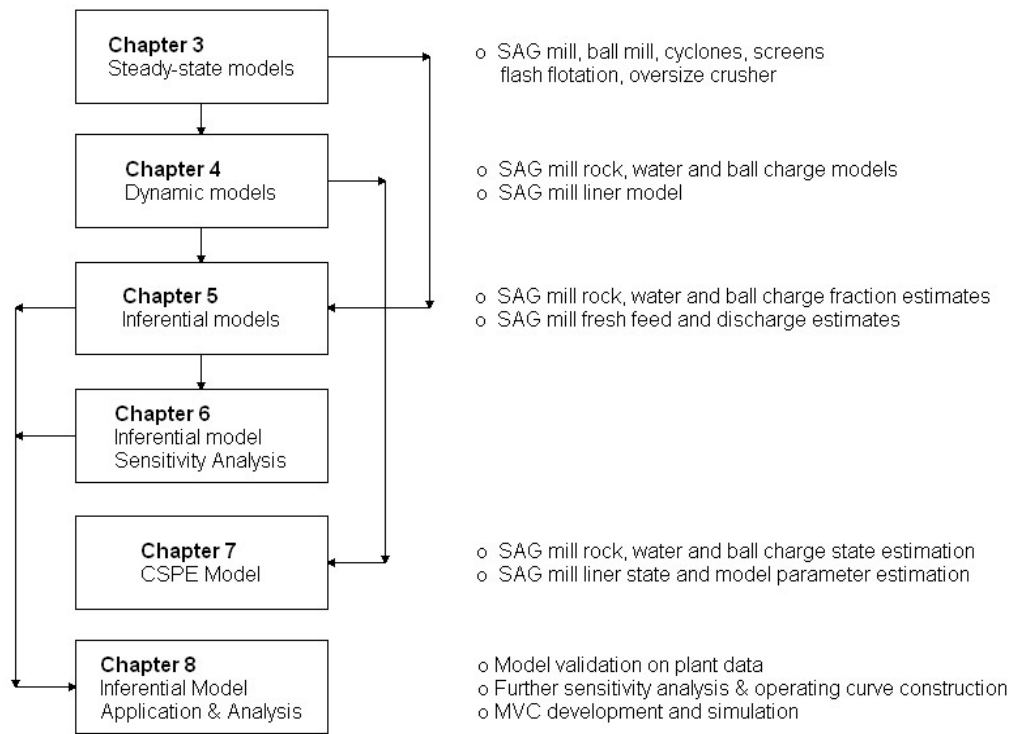

Figure 3.1: Model development logic, illustrating how the steady-state models form the foundation from which the dynamic, inferential and state-estimation are developed.

3.2   Model Validation Data Source

The data utilised for model validation originates from the results of detailed grinding circuit surveys conducted in early 1997 (David, 1997). A consultant from JKTech[1] attended site and co-ordinated the surveying of Module 1 and 2 grinding circuits with site personnel, including the author. Duplicate steady-state surveys of each grinding module were completed. The surveys were conducted for steady state model generation purposes.

The on-site survey procedure entailed:

1. **Setup:** Operating parameters conducive to steady-state grinding circuit operation were established a number of hours (nominally 4 hours in this case) prior to the target circuit survey start time. These operating parameters were maintained to allow the circuit to reach steady-state.

2. **Sampling:** Once steady-state conditions were prevalent, sampling of the circuit commenced. Fifteen−minute samples were taken of the primary and secondary cyclone feed, overflow and underflow streams, the SAG mill discharge screen undersize stream and the ball discharge stream over a two-hour period. Circuit operating parameters were monitored and recorded during this two-hour period to ensure steady-state conditions were maintained.

   The slurry-stream samples were collected using slotted, sampling scoops and collected in buckets. Cyclone feed sampling was effected by the utilisation of the periodic opening of the knife-gate valve feeding to a spare cyclone with a blanked-off overflow. This configuration allowed the taking of a feed sample via the cyclone spigot while the knife-gate valve was open.

3. **SAG mill crash-stop:** At the end of the two-hour survey period, the SAG mill was crashed-stopped. Once the SAG mill, SAG mill feed conveyor and the oversize crusher feed conveyor had been electrically isolated, belt-cut samples were taken and a mill inspection was completed to determine mill rock and ball loading. The belt-cut samples were collected into sealed, 44-gallon drums.

All of the samples were dispatched to The Julius Kruttschnitt Mineral Research Centre for size and moisture analysis. The results obtained were then utilised to generate *JKSimMet*[2] models for each of the processing unit operations, using the model-fitting functionality incorporated in *JKSimMet*. The individual models were then linked up to

---

[1]JKTech is the commercial division of the Julius Kruttschnitt Mineral Research Centre (JKMRC)

[2]Steady state mineral processing simulation software developed at the JKMRC and distributed by JKTech

match the topology of the Northparkes Mines grinding circuits. These circuit models were then used to simulate various operating conditions and process configuration alterations so that informed decisions regarding production targets were possible. The findings were documented in the report by David (1997), which was the main project deliverable.

The base-case simulation circuit model for Module 1 Grinding Circuit presented in the report represents the as-surveyed circuit model. It is this model that is used as the reference case for model validation in this document. As mentioned previously, the JKSimMet Module 1 circuit model results are detailed in Appendix B.

3.3   Steady State Model Development

This Section details steady state models of the following comminution unit operations:

- SAG mill
- hydrocyclones
- oversize crusher
- mill discharge screens
- ball mill
- flash flotation cells

The unit operation models have been coded into MATLAB-Simulink. The models are based on those developed by the Julius Kruttschnitt Mineral Research Centre (Morrell and Morrison, 1989; JKTech, 1994; Morrell and Delboni Jr, 1996; Morrell and Morrison, 1996; Napier-Munn *et al.*, 1996; Valery Jnr., 1998) with the model parameters being drawn from the survey models (David, 1997), see Appendix B.

The JKSimMet simulation model of the Module 1 grinding circuit is the basis of the model constructed in MATLAB-Simulink. The JKSimMet simulation results, model parameters and other grinding circuit survey data are contained in Appendix B. The JKSimMet simulation results also form the basis of the MATLAB-Simulink model validation.

In this Section, the unit operation models are firstly described with model validation of each unit operation in isolation. In Section 3.4 the units are linked together to simulate the Northparkes Mines Module 1 grinding circuit and validated against the survey information in Appendix B.

3.3.1 SAG Mill

A simplified cross-sectional view of the charge within a rotating SAG mill is shown in Figure 3.2. Lifter bars on the mill shell lift the charge to the shoulder from where the material is thrown or rolls (cataracts) towards the charge toe. The throwing, cataracting and general rubbing that occurs within the charge causes high energy (impact) and low energy (abrasion & attrition) breakage.

The rotating charge with the mill forms a kidney shape across which a velocity profile exists. At the 'eye' of the kidney the velocity is zero. The charge inner radius, r_i, delineates the "active" and "inactive" regions of the charge. Most breakage occurs within the active part of the charge and it is the active part of the charge that may be used in the modelling of mill weight and mill powerdraw.
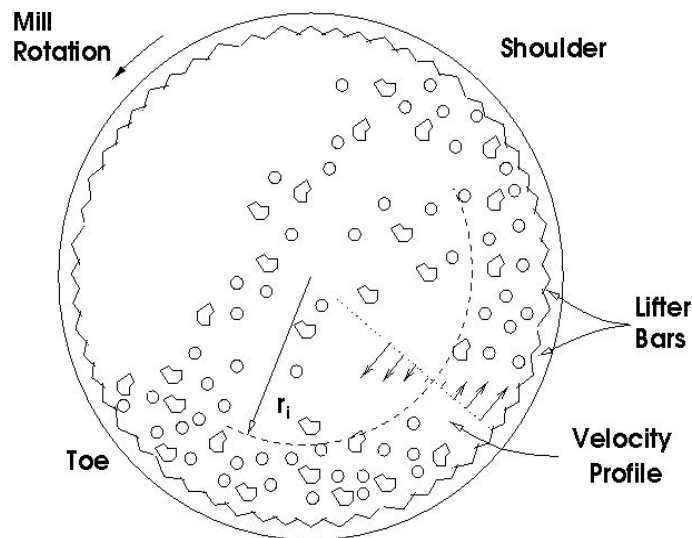

Figure 3.2: Simplified mill charge cross-section

The SAG mill model is comprised of:

1. solids balance

2. water balance

3. ball charge model

4. powerdraw model

5. impact zone model

The solids and water balances are inter-related and are integral to the perfectly mixed mill model described below. The ball charge model is independent of these mass balances.

However, the ball charge influences the solids balance via the breakage rates. The powerdraw and impact zone models are utilised once the mass balances and ball charge have been specified.

SAG Mill Charge/Product Model Algorithm

To further clarify the relationships between the mass balance and ball charge models, the calculation sequence for the perfectly mixed SAG mill model is presented below. Diagrammatic representation of this algorithm is given elsewhere (Napier-Munn *et al.*, 1996), (Valery Jnr., 1998).

1. Read input data

   - mill specifications
   - discharge grate specifications
   - general appearance function database
   - initial estimate of rock charge
   - ball charge
   - feedrate and size distribution
   - ore breakage characteristics
   - breakage rates

2. Make initial estimates of mill slurry holdup and mill discharge

3. Calculate low and high energy appearance functions and the combined appearance function

4. Apply the steady state perfectly mixed mill model

5. Compare the new estimates of mill slurry holdup with intial estimate

6. If error acceptable, stop

7. Else, adjust maximum discharge rate and return to Step 4.

Solids Balance

The solids mass balance for the SAG mill is based on the Whiten perfect mixing model (Whiten, 1974), which is an independently developed, special case of the general population balance model described elsewhere (Austin et al., 1987). On a size by size basis, the solids

may be stated as follows (Valery and Morrell, 1995), (Napier-Munn *et al.*, 1996):

$$Accumulation \quad = \quad In - Out + Generation - Consumption$$

$$\frac{ds_i}{dt} \quad = \quad f_i - p_i + \sum_{j=1}^{i-1} r_j s_j a_{ij} - (1 - a_{ii}) r_i s_i \tag{3.1}$$

$$Accumulation \quad = \quad 0 \; at \; steady \; state$$

$$0 \quad = \quad f_i - p_i + \sum_{j=1}^{i-1} r_j s_j a_{ij} - (1 - a_{ii}) r_i s_i \tag{3.2}$$

where

s_i	=	mill rock charge particles in *size i* (t)
f_i	=	feedrate of particles in *size i* (t/hr)
p_i	=	mill discharge (product) of particles in *size i* (t/hr)
r_i	=	breakage rate of particles in *size i* (hr^{-1})
a_{ij}	=	appearance function of particles appearing in *size i* (a function of the breakage distribution of particles in sizes $\geq$ *size i*) (fraction)

The feed component in Equation (3.1) requires no further discussion except that it is assumed to be known *e.g.*, from sizings of conveyor belt samples taken during a grinding survey. The product, generation and consumption components will now be discussed further.

Product

The mill product, p_i, (the SAG mill discharge stream, *SMDC*) is calculated as follows:

$$p_i = d_0 c_i s_i \tag{3.3}$$

where

d_0	=	maximum mill discharge rate constant (hr^{-1})
c_i	=	grate classification function for *size i* (fraction)
	=	probability of a *size i* particle passing through mill discharge grate

Referring to Equation (3.4) and Figure 3.3, the grate classification function, c_i, is equal to unity for particle sizes less than the size that behaves like water, x_m $(x < x_m)$ and equal to zero for particle sizes greater than the notional pebble port aperture size, x_p $(x > x_p)$. For particles sizes greater than the water-like size but less than or equal to the grate aperture size, x_g $(x_m < size \leq x_g)$, the classification function, c_i, decreases linearly to the point

$(x_g,\ f_p)$ where there is a change in gradient. From this point, the classification function, c_i, decreases linearly to the point $(x_p,0)$. The fitted model parameter f_p is the notional open area of the pebble ports as a fraction of the total grate open area (JKTech, 1994).

$$
\begin{aligned}
c_i &= 0.0 & \text{for } x \geq x_p \\
c_i &= \frac{x_p - x}{x_p - x_g} f_p & \text{for } x_g < x < x_p \\
c_i &= \frac{x - x_m}{x_g - x_m}(f_p - 1) + 1.0 & \text{for } x_m < x \leq x_g \\
c_i &= 1.0 & \text{for } x \leq x_m
\end{aligned}
\tag{3.4}
$$
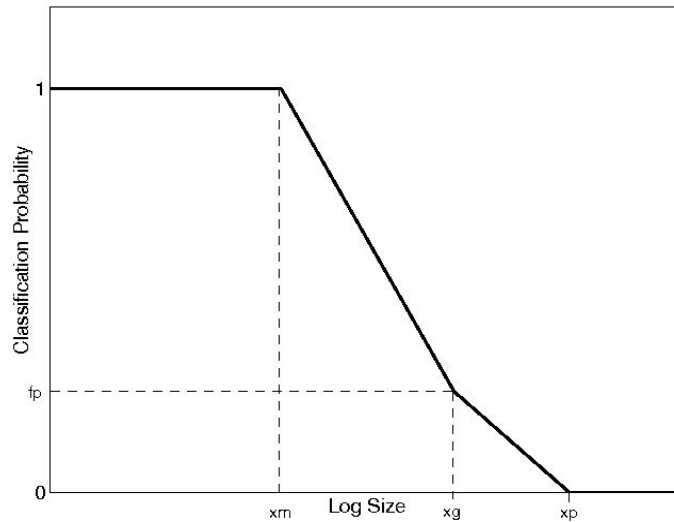
Figure 3.3: Grate Classification Function

The mill ore charge, s_i, product, p_i, and maximum mill discharge rate constant, d_0 are determined in an iterative manner given the initial estimate of the ore charge and x_m, the particle size which behaves effectively as water in the mill.

From the initial estimates of the SAG mill rock charge properties $(SMRC)$ and size distribution $(smrc)$ the volumetric fraction of the grinding charge occupied by slurry, J_{pm}, is determined which can then be utilised to determine the volumetric discharge from the mill, Q.

$$Q \;=\; Q_m \;+\; Q_t \tag{3.5}$$

$$Q_m \;=\; 6100\, J_{pm}^2 \gamma^{2.5} A \phi^{-1.38} D^{0.5} \tag{3.6}$$

$$Q_t \;=\; 935\, J_{pt} \gamma^2 A\, D^{0.5} \tag{3.7}$$

where

Q_m = mill discharge flowrate through grinding media (m^3/hr)

Q_t = mill discharge flowrate through slurry pool at toe of the charge (m^3/hr)

A = total discharge grate open area (m^2)

D = mill inside diameter (m)

γ = mean relative radial position of open area (fraction)

ϕ = fraction critical mill speed (fraction)

$$J_{max} \;=\; 0.5\, J_t \;-\; J_{po} \tag{3.8}$$

= maximum possible nett fractional grinding media slurry holdup (fraction)

$$J_p \;=\; J_{pg} \;-\; J_{po} \tag{3.9}$$

$$\;=\; J_{pm} \text{ (for } \mathrm{J}_p \leq \mathrm{J}_{max}) \tag{3.10}$$

$$\;=\; J_{pt} \;+\; J_{pm} \text{ (for } \mathrm{J}_p > \mathrm{J}_{max}) \tag{3.11}$$

= nett fractional holdup of slurry in mill (fraction)

J_{pm} = nett fractional holdup of slurry in mill that is contained within

the grinding charge interstices (fraction)

J_{pt} = nett fractional holdup of slurry in mill that is contained in

the slurry pool at the toe of the charge (fraction)

(*i.e.*, slurry outside the grinding charge)

J_{pg} = gross fractional holdup of slurry in mill (fraction)

$$J_{po} \;=\; 0.33(1 \;-\; r_n) \tag{3.12}$$

= nett fractional slurry holdup in mill 'dead' zone (fraction)

(*i.e.*, fraction of mill volume outside outermost grate apertures)

$$J_{pt} \;=\; J_p \;-\; J_{max} \tag{3.13}$$

J_t = mill volume fraction occupied by the grinding charge

(balls + coarse rocks + interstices) (fraction)

r_n = relative radial position of outermost grate apertures (fraction)

The initial estimates of volumetric mill discharge and rock charge are used to determine the the maximum mill discharge rate, d_0 (Valery Jnr., 1998),

$$d_0 = \frac{Q_m + Q_t}{(J_{pm} + J_{pt}) \cdot V_m} \tag{3.14}$$

where

$$V_m \quad = \quad \text{mill internal volume (m}^3)$$

Napier-Munn et $al.$ (1996) state that the charge toe angle, θ_T, and the slurry toe angle, θ_{TO}, are equal for grate discharge mills, $i.e.$,

$$\theta_{TO} = \theta_T \tag{3.15}$$

This implies that no slurry pool exists and the nett fractional hold up of slurry is less than the media maximum holdup capacity, $i.e.$, $J_p \leq J_{max}$, and reduces Equation (3.14) to

$$d_0 = \frac{Q_m}{J_{pm} \cdot V_m} \tag{3.16}$$

and mill volumetric discharge may then be calculated from Q_m only (Equation (3.6)). (Section 3.3.1 discusses charge toe and slurry toe angle in more detail.)

Recognising the the mill volumetric discharge, Q_m, is in fact the mill product which consists of water and water-like solids ($size < x_m$), $i.e.$,

$$p_{xm} = k_g Q_m \tag{3.17}$$

allows the calculation of an initial estimate of the maximum discharge rate constant, d_0, and the volume of solids of $size < x_m$, s_{xm}, from

$$d_{xm} \quad = \quad \frac{p_{xm}}{s_{xm}} \tag{3.18}$$

where

$$d_{xm} \quad = \quad d_0 \tag{3.19}$$

$$= \quad \text{mill discharge rate for water and solids of size} < x_m \text{ (hr}^{-1})$$

$$= \quad \text{maximum mill discharge rate constant (hr}^{-1})$$

$$s_{xm} \quad = \quad J_{pg} \, \pi \, \frac{D_m^{\;2}}{4} L_m \tag{3.20}$$

$$= \quad \text{volume of water and solids of size} < x_m \text{ in the mill (m}^3)$$

$$k_g \quad = \quad \text{factor to account for coarse material } (-)$$

The steady state mass balance, Equation (3.1), is then applied and solved for the rock load, $SMRC/smrc$. The corresponding volume of rock load smaller than x_m is then calculated

and compared to the initial estimate. The maximum discharge rate, d_0, is adjusted by Equation (3.21) until agreement is satisfactory.

$$d_{0,\ k+1} = d_{0,\ k} \cdot \frac{s_{xm,\ k+1}}{s_{xm,\ k}} \tag{3.21}$$

where

$d_{0,\ k+1}$ =   discharge rate constant at $k\ +\ 1^{th}$ iteration (hr^{-1})

$d_{0,\ k}$ =   discharge rate constant at k^{th} iteration (hr^{-1})

$d_{0,\ k+1}$ =   discharge rate constant at $k\ +\ 1^{th}$ iteration (hr^{-1})

$s_{xm,\ k+1}$ =   mill water and rock charge smaller than x_m at $k\ +\ 1^{th}$ iteration (m^3)

$s_{xm,\ k}$ =   mill water and rock charge smaller than x_m at k^{th} iteration (m^3)

k =   iteration step

In summary, the calculation sequence for the maximum mill discharge rate constant (d_0) is as follows:

1. Given

    - initial estimates of the rock charge, $SMRC/smrc$
    - particle size that behaves effectively as water, x_m

    determine

    - volumetric fraction of grinding charge voidage occupied by slurry, J_{pm}
    - the mill volumetric discharge (product), $k_g Q_m = p_{xm}$
    - the volume of slurry within the mill, s_{xm}
    - the discharge rate for water and sub x_m size solids (maximum discharge rate constant), $d_{xm} = d_0$

2. apply steady state mass balance and solve for mill rock charge, s_i

3. recalculate s_{xm} and compare to initial estimate

4. if agreement is within tolerance, stop

5. else, adjust d_0 and goto Step 2.

Consumption and Generation

Both the generation and consumption components have a dependence on the breakage rate function, r_i, and the appearance function, a_{ij}.

Breakage Rate Function, r_i :   The "variable rates model" (JKTech, 1994) and (Morrell and Morrison, 1996) is a set of five pairs of "knot" sizes and base breakage rates. The knot sizes are selected to encompass the size distribution and capture important features of the breakage rate curve, *e.g.*, the slower breaking rates of the critically sized material (which is discharged from the mill via pebble ports and recycled to the oversize crusher). The breakage rate for each particle size is determined by interpolation. The base breakage rates are as follows (JKTech, 1994) and (Morrell and Morrison, 1996):

$$ln(R1) \;=\; \frac{(k_{11} + k_{12}ln(R2) - k_{13}ln(R3) + J_B(k_{14} - k_{15}F_{80}) - D_B)}{S_b} \tag{3.22}$$

$$ln(R2) \;=\; k_{21} + k_{22}ln(R3) - k_{23}ln(R4) - k_{24}F_{80} \tag{3.23}$$

$$ln(R3) \;=\; S_a + \frac{(k_{31} + k_{32}ln(R4) - k_{33}R_r)}{S_b} \tag{3.24}$$

$$ln(R4) \;=\; S_b\,((k_{41} + k_{42}ln(R5) + J_B\,(k_{43} - k_{44}F_{80}) \tag{3.25}$$

$$ln(R5) \;=\; S_a + S_b\,(k_{51} + k_{52}F_{80} + J_B\,(k_{53} - k_{54}F_{80}ln(R4)) - 3D_B) \tag{3.26}$$

where

$R1 \ldots R5$ =   base breakage rates (hr^{-1})

k_{ij} =   regression coefficients

J_B =   mill volume occupied by grinding balls and associated voids (%)

$$S_a \;=\; ln(\frac{RPM}{23.6}) \tag{3.27}$$
   =   mill RPM scaling factor

$$S_b \;=\; ln(\frac{N_{fcs}}{0.75}) \tag{3.28}$$
   =   mill fraction critical speed scaling factor

$$D_B \;=\; ln(\frac{D_{ball}}{90}) \tag{3.29}$$
   =   ball topsize scaling factor

$$R_r \;=\; \frac{\text{tph recycled material } -20 + 4 \text{ mm}}{(\text{tph fresh feed + tph recycled material } -20 + 4 \text{ mm })} \tag{3.30}$$
   =   recycle ratio of $-20 + 4$ mm material

Regression coefficients, k_{ij}, are given in Table 3.1 and are based on data collected by the Julius Kruttschnitt Mineral Research Centre. From inspection of Equations (3.22) through (3.30) it is evident that the breakage rates are a function of:

- equipment parameters (mill speed and ball size)

- parameters (regression coefficients)

- operating conditions (feed size, recycle ratio and ball charge level, J_b)

Detail of the effects of ball load, feed size, recycle load, mill speed and ball size on the breakage rates can be found elsewhere (Morrell and Morrison, 1996).

Table 3.1: Breakage Rate Regression Coefficients, k_{ij}

j	k_{1j}	k_{2j}	k_{3j}	k_{4j}	k_{5j}
1	2.504	4.682	3.141	1.057	1.894
2	0.397	0.468	0.402	0.333	0.014
3	0.597	0.327	4.632	0.171	0.473
4	0.192	0.0085	-	0.0014	0.002
5	0.002	-	-	-	-

Appearance Function, a_{ij} : The appearance function, a_{ij}, is a matrix of column vectors that describe:

1. the amount of material in a give size that is "selected" for breakage, and,

2. the distribution that remains after breakage has occurred

Each particle size has its own vector and thus, the appearance function matrix is a square matrix of dimension (no. of sizes $\times$ no. of sizes). Since there is no particle growth, the appearance function matrix is a lower-triangular matrix.

Each appearance function vector is a weighted average of high-energy (impact) breakage and low-energy (abrasion) breakage appearance functions:

$$a_{ij} = \frac{t_{le}a_{le} + t_{he}a_{he}}{t_{le} + t_{he}} \qquad (3.31)$$

where

$$
\begin{aligned}
a_{he} &= \text{high energy appearance function, (fraction)} \\
a_{le} &= \text{low energy appearance function (fraction)} \\
t_{he} &= \text{high energy (impact) } t \text{ parameter (\%)} \\
t_{le} &= \text{low energy (abrasion) } t \text{ parameter (\%)}
\end{aligned}
$$

The t parameters are size distribution data identifiers, $i.e.$, a look-up table reference point for data in a Julius Kruttschnitt Mineral Research Centrereference database. The high energy t parameter is also known as the "$t10$" or "t_{10}" parameter and the low energy t parameter is also known as the "ta" or "t_a" parameter. That is,

$$
\begin{aligned}
t_{10} &= t_{he} \\
t_a &= t_{le}
\end{aligned}
\qquad (3.32)
$$

Breakage due to abrasion is assumed to be independent of size. For a given ore type a t_a value is determined from laboratory abrasion tests. The t_a is the cummulative percent (by weight) of material passing $\frac{1}{10}th$ of the original particle size after low energy breakage has occurred. For example, a 30mm particle with a $t_a = 1\%$ is subjected to a low energy breakage event after which 1% of the material is < 3 mm in size. That is, mostly large particles remain, as expected for abrasion breakage. A complete distribution is obtained from a single t_a value from Table 3.3.1.

Table 3.2: Low Energy Appearance Function

Particle Size (t value)	Cummulative % Passing (t_a scaling factor)
$t_{1.25}$	$2.687 \cdot t_a$
$t_{1.5}$	$1.631 \cdot t_a$
t_{10} (t_a)	$1.0 \cdot t_a$
t_{100}	$0.9372 \cdot t_a$
t_{250}	$0.8070 \cdot t_a$
t_{500}	$0.6365 \cdot t_a$

p A-74 Appendix A9 (JKTech, 1994)

The cummulative percent passing distribution of the particle sizes of interest are determined by interpolation. Conversion to a weight fraction retained format results in the low energy appearance function.

Breakage due to impact is dependent on ore type and on the particle size (by way of the breakage energy that is exerted on particles of that size). Therefore, each size fraction has a unique t_{10} value.

A t_{10} value is the cummulative percent (by weight) of material passing $\frac{1}{10}th$ of the original particle size after high energy breakage has occurred. A complete distibution is obtained from a single t_{10} value from a database of t_{10} *versus* $[t_{75}, t_{50}, t_{25}, t_4, t_2]$ data. Again, the cummulative percent passing distribution of the particle sizes on interest are determined by interpolation.

The ore dependancy is determined from laboratory test work and is reported as two impact breakage parameters, A and b. The breakage energy dependancy is through a specific comminution energy, Ecs, parameter. The t_{10} values for each size fraction is determined

using these three parameters (A, b, Ecs) as follows:

$$t_{10_i} = A\,(1 - e^{-b\,Ecs_i})$$ (3.33)

where

A $=$ ore impact breakage parameter ($-$)

b $=$ ore impact breakage parameter ($-$))

Ecs_i $=$ specific comminution energy for $size\ i$ (kWhr/t)

The specific comminution energy, Ecs_i, is a vector of the amount of energy available for impact breakage of the $i\,th$ particle size and is determined as follows (Valery Jnr., 1998):

$$Ecs_i = \frac{\psi_e\,gms_i\,\rho_{m_i}\,g\,h}{SG_s\,x_i\,3.6 \times 10^3}$$ (3.34)

where

ψ_e $=$ energy absorption factor of the steel grinding media (fraction)

gms_i $=$ grinding media size class i (mm)

ρ_{m_i} $=$ density of grinding media in $size\ i$ (t/m^3)

g $=$ gravitational acceleration (m/s^2)

h $=$ mean drop height (m)

SG_s $=$ ore specific gravity (t/m^3)

x_i $=$ target particle $size\ i$ (mm)

3.6×10^3 $=$ $\frac{kWhr}{t}$ conversion factor

The mean drop height, h, is determined from charge geometry information as follows:

$$h = \frac{(r_{sm} + r_i)}{2}\,(\,sin(\theta_S) - sin(\theta_T)\,)$$ (3.35)

where

r_{sm} $=$ SAG mill radius (m)

r_i $=$ SAG mill charge inner radius (m)

θ_S $=$ SAG charge shoulder angle (radians) (see Section 3.3.1)

θ_T $=$ SAG charge toe angle (radians) (see Section 3.3.1)

The target particle size, x_i, is the geometric mean of the size distribution intervals, $i.e.$,

$$x_i = \frac{(\,size_{i-1} + size_i)}{2}$$ (3.36)

The density of grinding media in $size\ i$, ρ_{m_i}, is calculated as follows (Valery Jnr., 1998):

$$\rho_{m_i} = \frac{(\frac{1}{2}\,vo_i\ +\ \sum_{i=1}^{i-1}\,vo_i)\,SG_s\ +\ (\sum_{i=1}^{n}\,vb_i)\,SG_b}{\frac{1}{2}\,vo_i\ +\ \sum_{i=1}^{i-1}\,vo_i\ +\ \sum_{i=1}^{n}\,vb_i} \tag{3.37}$$

where

$$
\begin{aligned}
i\quad &=\quad \sqrt{2}\ \text{size class} \\
&\qquad i\ =\ 1\ :\ \text{largest size} \\
&\qquad i\ =\ n\ :\ \text{smallest ball size} \\
&\qquad i\ =\ q\ :\ \text{smallest rock size (16 mm)} \\
&\qquad i\ =\ z\ :\ \text{smallest particle size} \\
vo_i\quad &=\quad \text{the volume of ore in size class } i\ (\text{m}^3) \\
vb_i\quad &=\quad \text{the volume of grinding balls in size class } i\ (\text{m}^3) \\
SG_b\quad &=\quad \text{grinding ball density } (\text{t/m}^3)
\end{aligned}
$$

Grinding balls and ore larger than fifty 50 mm constitutes grinding media. Fifty percent of rock in $size\ i$ is larger than the remaining fifty percent and can theoretically cause breakage within the size fraction. All rocks greater in size than $size\ i$ and all of the grinding balls can cause breakage. Therefore, the grinding media size that is effective on $size\ i$, gms_i, is calculated as follows (Valery Jnr., 1998):

$x_i\ \geq\ 50\,mm$

$$gms_i\quad =\quad \left(\frac{\frac{1}{2}\,n_i\,x_i^2\ +\ \sum_{j=1}^{i-1}\,n_j\,x_i^2\ +\ \sum_{j=1}^{z}\,nb_j\,x_j^2}{\frac{1}{2}\,n_i\ +\ \sum_{j=1}^{i-1}\,n_j\ +\ \sum_{j=1}^{z}\,nb_j}\right)^{0.5} \tag{3.38}$$

$x_i\ <\ 50\,mm$

$$gms_i\quad =\quad gms_{i-1}$$

where

$$n_i\quad =\quad \frac{SMRC_i}{M_i} \tag{3.39}$$
$$= \text{number of particles in } size\ i$$

$$SMRC_i\quad = \text{SAG mill rock charge mass in } size\ i\ (\text{t})$$

$$M_i\quad =\quad \frac{\pi}{6}\left(\frac{size}{1\times10^3}\right)^3\,SG_s \tag{3.40}$$
$$= \text{mass of an ore particle in } size\ i\ (\text{t})$$

$$nb_i\quad =\quad \frac{SMBC_i}{Mb_i} \tag{3.41}$$
$$= \text{number of grinding balls in } size\ i$$

$$SMBC_i\quad = \text{SAG mill ball charge mass in } size\ i\ (\text{t})$$

$$Mb_i\quad =\quad \frac{\pi}{6}\left(\frac{size}{1\times10^3}\right)^3\,SG_b \tag{3.42}$$
$$= \text{mass of grinding ball in } size\ i\ (\text{t})$$

The energy absorption factor of the steel grinding media, ψ_e, which reduces the energy imparted to rock breakage due to the elastisticity of the grinding balls, is determined as follows (Valery Jnr., 1998):

$$\psi_e \;=\; \frac{(\sum_{i=1}^{z} vb_i)\, SG_b \;+\; (\sum_{i=1}^{q} vo_i)\, SG_s}{(\sum_{i=1}^{q} vo_i)\, SG_s} \tag{3.43}$$

In summary, the determination of the appearance function, a_{ij}, involves the following steps:

1. Laboratory determination of A, b and t_a

2. Calculation of the abrasion appearance function by interpolation of the particle size distribution into the data in Table 3.3.1

3. Calculation of the impact appearance function by calculating:

   (a) the specific comminution energy, Ecs_i, from Equation (3.34) through Equation (3.43)

   (b) the t_{10} values for each size fraction from Equation (3.33)

   (c) the impact appearance function for each size fraction by interpolation against Julius Kruttschnitt Mineral Research Centre data

   (d) the appearance function in fraction retained format

4. Calculation of the (combined) appearance function, a_{ij}, - a weighted average of the high and low energy appearance functions - from Equation (3.31)

With the appearance function, a_{ij}, and the breakage rates, r_i, determined, the generation and consumption terms of the solids mass balance, Equation (3.1), may be calculated.

Consumption, $(1 \;-\; a_{ii})r_i s_i$ **:** Recalling that the appearance function, a_{ij} is in a mass fraction retained format, the diagonal of the appearance function, a_{ii}, indicates (by difference) how much of the material in a given size is broken and distributed into the size fractions below (according to the appearance function for that given parent size).

Generation, $\sum_{j=1}^{i-1} r_j s_j a_{ij}$ **:** Summation of the product of the rock charge mass in the size fractions above *size i*, s_j, and their respective breakage rates, r_j, and the fraction appearing into *size i* from the breakage occurring above, a_{ij}, results in the generation term for *size i*.

The feed, product, consumption and generation terms are now determined and the mass balance, Equation (3.1), is now defined.

Water Balance

As is evident from the discussion about mill product, p_i, earlier in this Section, the solids and water balance are interlinked via the volumetric discharge flowrate (Q_m) and the maximum discharge rate constant (d_0). With zero consumption and generation, the water mass balance is as follows:

$$
\begin{aligned}
Accumulation &= In - Out \\
\frac{ds_w}{dt} &= f_w - p_w \\
\text{where} & \\
s_w &= \text{water in the mill charge (t)} \\
f_w &= \text{feed water addition (t/hr)} \\
p_w &= \text{water discharge rate (t/hr)} \\
&= d_0 \ s_w
\end{aligned}
$$

(3.44)

(3.45)

The water balance calculation sequence is as follows:

1. the feedwater addition rate is specified

2. the water discharge rate is calculated from Equation (3.45), and,

3. the mill water charge is calculated from Equation (3.44).

Ball Charge Model

The ball charge model is essentially a user specified ball charge volume and size distribution. There are no "In", "Out", "Generation", "Consumption", or, "Accumulation" terms. The user specifies the:

- ball charge volumetric load, J_b

- ball topsize

- ball size distribution (four size fractions)

  see Table 3.3 for example.

Table 3.3: SAG Mill Ball Charge Model

Ball Load Fraction, J_b	(fraction)	0.14

Ball Top Size	(mm)	125
Size 1: Top Size$\times \frac{1}{\sqrt{2}}$	(%)	50
Size 2: Top Size$\times \frac{1}{2}$	(%)	35
Size 3: Top Size$\times \frac{1}{2\sqrt{2}}$	(%)	15
Size 4: Top Size$\times \frac{1}{4}$	(%)	0

Powerdraw Model

According to the Morrel powerdraw model (Morrell, 1994), the mill powerdraw, P_{Gross}, is as follows:

$$P_{Gross} = P_{No\,Load} + kP_{Charge} \tag{3.46}$$

where

$P_{No\,Load}$	=	no-load power of mill (empty mill powerdraw) (kW)
P_{Charge}	=	mill powerdraw attributable to the entire contents of the mill (kW)
k	=	mill powerdraw lumped parameter (accounts for heat losses due to internal friction, energy of attrition/abrasion breakage, rotation of the grinding media and inaccuracies in assumptions and charge shape and motion measurements (dimensionless)

The no-load component of the mill powerdraw, $P_{No\,Load}$ is,

$$P_{No\,Load} = 1.68 \left(D_m{}^{2.5} \phi_{fcs} \left(0.667\,L_{cone} + L_m \right) \right)^{0.82} \tag{3.47}$$

where

D_m	=	mill inside diameter (m)
ϕ_{fcs}	=	mill fraction critical speed (fraction)
L_{cone}	=	length of the conical section of the mill (m)

The powerdraw component attributable to mill charge contents, P_{Charge}, consists of components of powerdraw attributable to material in the conical feed end section of the mill

and the material in the cylindrical section of the mill, as shown in Equation (3.48).

$$P_{Charge} = P_{Net} + P_{Cone} \tag{3.48}$$

where

P_{Net} = mill powerdraw attributable to the contents of the cylindrical
section of the mill (kW)

P_{Cone} = mill powerdraw attributable to the contents of the conical
(feed) section of the mill (kW)

The powerdraw attributable to the cylindrical and conical sections of the mill are determined by Equation (3.49) and Equation (3.50), respectively.

$$
\begin{aligned}
P_{Net} =\ & \frac{\pi\, g L_m N_m\, r_m \left(2\, r_m{}^3 - 3\, z r_m{}^2 r_i + r_i{}^3\, (3\, z - 2)\right) \left(\rho_c \left(\sin(\theta_S) - \sin(\theta_T)\right)\right)}{3\, r_m - 3\, z r_i} \\
& + \frac{\pi\, g L_m N_m\, r_m \left(2\, r_m{}^3 - 3\, z r_m{}^2 r_i + r_i{}^3\, (3\, z - 2)\right) \left(\rho_p \left(\sin(\theta_T) - \sin(\theta_{TO})\right)\right)}{3\, r_m - 3\, z r_i} \\
& + \frac{L_m \rho_c\, N_m{}^3 r_m{}^3 \pi^3 \left((r_m - z r_i)^4 - r_i{}^4\, (z - 1)^4\right)}{(r_m - z r_i)^3}
\end{aligned} \tag{3.49}
$$

$$
\begin{aligned}
P_{Cone} =\ & \frac{\pi\, g L_{cone}\, N_m \left(r_m{}^4 - 4\, r_m\, r_i{}^3 + 3\, r_i{}^4\right) \left(\rho_c \left(\sin(\theta_S) - \sin(\theta_T)\right)\right)}{3\,(r_m - r_t)} \\
& + \frac{\pi\, g L_{cone}\, N_m \left(r_m{}^4 - 4\, r_m\, r_i{}^3 + 3\, r_i{}^4\right) \left(\rho_p \left(\sin(\theta_T) - \sin(\theta_{TO})\right)\right)}{3\,(r_m - r_t)} \\
& + 2\, \frac{2\, \pi^3 N_m\, L_{cone}\, \rho_c \left(r_m{}^5 - 5\, r_m\, r_i{}^4 + 4\, r_i{}^5\right)}{5\,(r_m - r_t)}
\end{aligned} \tag{3.50}
$$

where

g = gravitational acceleration (9.81 m/s^2)

L_{cone} = length (axial) of conical section of mill (m)

L_m = length of the cylindrical section of the mill (m)

N_m = actual mill speed (revolutions per second)

P_{Cone} = mill powerdraw attributable to the contents of the conical
(feed) section of the mill (kW)

r_i = mill charge surface inner radius (m)

r_m = mill radius (m)

r_t = mill trunnion radius (m)

z = mill powerdraw calculation parameter $(-)$

ρ_c = mill charge density (specific gravity) (t/m^3)

ρ_p = mill pulp density (specific gravity) (t/m^3)

θ_S = mill charge shoulder angle (radians), see Figure 3.4

θ_T = mill charge toe angle (radians), see Figure 3.4

θ_{TO} = mill slurry toe angle (radians), see Figure 3.4

The mill pulp density, ρ_p, is assumed to be equal to the mill discharge pulp density:

$$\rho_p = SMDC_{SGp} \tag{3.51}$$

where

ρ_p = SAG mill pulp density (t/m^3)

$SMDC_{SGp}$ = SAG mill discharge pulp density (t/m^3)

Mill cone length is determined as follows:

$$L_{cone} = \frac{(D_m - D_t)}{2} \tan(\frac{\pi}{180}\,\theta_{cone}) \tag{3.52}$$

where

L_{cone} = length (axial) of conical section of mill (m)

D_m = mill inside diameter (m)

θ_{cone} = mill cone angle $(^o)$

Figure 3.4 shows a simplified mill charge geometry (is cross-section). The 'C' or kidney shape describes the surface of the "active" part of the charge where particle breakage occurs. Figure 3.4 also shows the charge shoulder angle (θ_S), charge toe angle (θ_T), and the charge inner surface radius (r_i) which define the charge geometry.

The angle of the mill charge shoulder, θ_S, is given by:

$$\theta_S = \frac{\pi}{2} - (\theta_T - \frac{\pi}{2})\left((0.3386 + 0.1041\,\phi_{fcs}) + (1.54 - 2.5673\,\phi_{fcs})\,J_t\right) \tag{3.53}$$

The angle of the mill charge toe, θ_T is given by:

$$\theta_T = 2.5307\,(1.2796 - J_t)\left(1 - e^{-19.42\,(\phi_c - \phi_{fcs})}\right) + \frac{\pi}{2} \tag{3.54}$$

Since the SAG mill is a grate discharge mill, the angle of the mill charge slurry toe, θ_{TO} is equal to the charge to angle:

$$\theta_{TO} = \theta_T \tag{3.55}$$
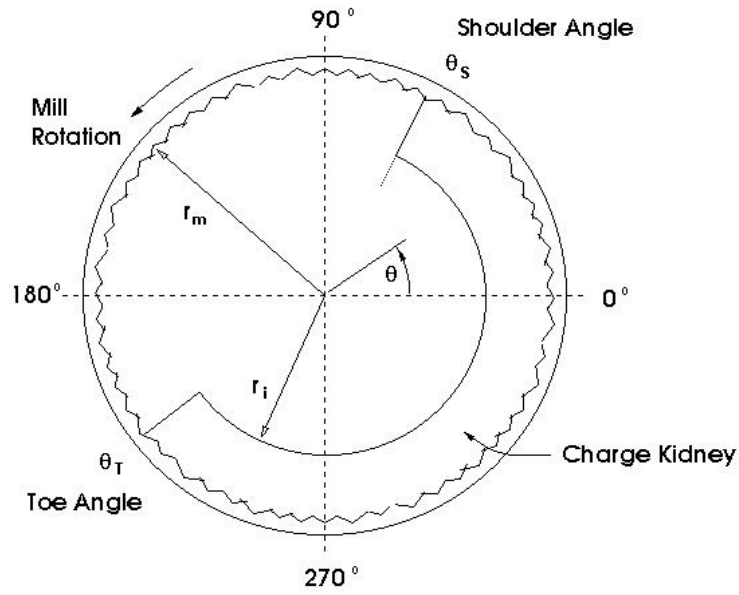
Figure 3.4: Simplified mill charge geometry

The powerdraw calculation parameter, z, is given by:

$$z = (1 - J_t)^{0.4532} \qquad (3.56)$$

Mill critical speed, $RPM_{critical}$, (the rotational speed where angular acceleration is equal to gravitational acceleration) is as follows:

$$RPM_{critical} = \frac{60}{2\pi} \sqrt{\frac{2g}{D_m}} \qquad (3.57)$$

The actual mill speed, represented as a fraction of the critical speed, ϕ_{fcs}:

$$\phi_{fcs} = \frac{RPM}{RPM_{critical}} \qquad (3.58)$$

where

RPM = actual mill speed (revolutions per minute)

The actual mill speed in revolutions per second, N_m is:

$$N_m = \frac{RPM}{60} \qquad (3.59)$$

The mean rotational rate, $\overline{N}$, is given by:

$$\overline{N} = \frac{N_m}{2} \tag{3.60}$$

The mill charge density, ρ_c, is determined as follows:

$$\rho_c = \frac{\left(J_t\,\rho_o\,\left(1 - \epsilon + \epsilon U \frac{S}{100}\right) + J_b\,(\rho_b - \rho_o)\,(1 - \epsilon) + J_t\,\epsilon U\left(1 - \frac{S}{100}\right)\right)}{J_t} \tag{3.61}$$

where

J_b	$=$	mill fraction occupied by grinding balls including the associated voidage (fraction mill volume)
S	$=$	mill discharge volumetric solids content (% solids v/v)
ϵ	$=$	mill charge porosity (fraction)
ρ_b	$=$	grinding ball density (specific gravity) (t/m^3)
ρ_c	$=$	mill charge density (specific gravity) (t/m^3)
ρ_o	$=$	ore density (specific gravity) (t/m^3)

The fraction of grinding media voidage occupied by the slurry, U, is:

$$U = \frac{J_{pm}}{\epsilon J_t} \tag{3.62}$$

The remaining variables yet to be defined are: ϕ_c, t_c, t_f, β, $\overline{r}$ and r_i.

The experimentally determined fraction of critical mill at which centrifuging is fully established, ϕ_c, is calculated as follows:

$$\phi_c = 0.35\,(3.364 - 0.35\,J_t) \tag{3.63}$$

The mean travel time for material in the charge (from the charge toe to the charge shoulder), t_c, is:

$$t_c = \frac{2\,\pi - \theta_T + \theta_S}{2\pi\,\overline{N}} \tag{3.64}$$

The mean travel time for material in free fall (from the charge shoulder to the charge toe), t_f, is:

$$t_f = \left(\frac{2\overline{r}\,(\sin(\theta_S) - \sin(\theta_T))}{g}\right)^{0.5} \tag{3.65}$$

The fraction of charge that is active, β, is determined as follows:

$$\beta = \frac{t_c}{t_f + t_c} \tag{3.66}$$

The mean radial position of the mill charge, $\bar{r}$, is calculated as follows:

$$\bar{r} = \frac{r_m}{2} \left(1 + \left(1 - \frac{2\pi J_t}{2\pi - \theta_T + \theta_S} \right)^{0.5} \right) \tag{3.67}$$

The radial position of the mill charge inner surface, r_i, can then be determined:

$$r_i = r_m \left(1 - \frac{2\pi \beta J_t}{2\pi - \theta_T + \theta_S} \right)^{0.5} \tag{3.68}$$

All parameters and variables in the model are now specified and mill powerdraw may now be calculated by Equation (3.46).

Impact Zone Model

Although the mill considered in this research is a fixed speed mill, variable speed mills are becoming increasingly popular. The mill speed affects the

1. breakage rates, r_i (see Equations (3.22) to (3.26))

2. volumetric discharge, Q_m (see Equation (3.6))

3. mill powerdraw, P_{Gross} (see Equations (3.49) & (3.50))

4. charge shape as defined by the

   - toe angle, θ_T (see Equation (3.54))
   - shoulder angle, θ_S (see Equation (3.53))
   - active charge radius, r_i (see Equation (3.68))

An important implication of the charge shape is the location of the impact zone. For a fixed speed mill, the impact zone is designed to be on the toe of the charge. When the mill is powered by a variable speed drive, the impact zone can move between a point within the charge to a point beyond the toe of the charge. In the latter case, damage to the mill liners and lifter bars is caused by the direct impact of grinding balls.

Since such conditions are undesirable, a model for locating the impact zone has been included in the SAG mill model. Although a ball trajectory model is not part of the DOS based JKSimMet simulation software (Version 4), a trajectory model has since been incorporated into the succeeding Microsoft Windows based version (Schroder, 2000). The exact details of the model were not available at the time of coding the MATLAB-Simulink models, however, it is believed to be based on the equations for projectile motion. Thus, a simple model for the point of impact is proposed here that utilises projectile motion equations.

Projectile Motion Equations

The equations governing the motion of projectiles are those of constant acceleration (Alonso and Finn, 1969):

$$v_1 = v_0 + at \tag{3.69}$$

$$s_1 = s_0 + v_0 t + \frac{1}{2}at^2 \tag{3.70}$$

where

a	=	acceleration (m/s^2)
v	=	velocity (m/s)
s	=	distance (m)
t	=	time (sec)
0	=	initial conditions
1	=	conditions at time t

The motion is analysed in the horizontal plane (where acceleration is zero, *i.e.*, $a_h = 0$), denoted with a subscript 'h', and the vertical plane (where acceleration is due to gravity, *i.e.*, $a = -g = -9.81$ m/s^2), denoted with a subscript 'v'. The analysis is divided into the upward the downward motion. The initial conditions of the motion in this instance are those of the charge shoulder and are denoted with a subscript zero, *e.g.*, v_{0h} for initial horizontal velocity. The end of the upward journey and beginning of the downward journey is denoted with a subscript one, *e.g.*, v_{1h} for horizontal velocity at maximum projectile height. The final conditions of the downward journey, at the point of impact, are denoted with a subscript two, *e.g.*, v_{2h} for horizontal velocity at the point of impact with the mill shell.

Using the central axis of the mill as the reference point and the horizontal axis positive sense pointing to the side of the mill ofthe charge shoulder, the equations of motion are

UP

Horizontal

$$v_{0,h} = -\frac{RPM}{60} 2r_m\pi\cos(\theta_S) \tag{3.71}$$

$$v_{1,h} = v_{0,h} \tag{3.72}$$

$$s_{0,h} = r_m\cos(\theta_S) \tag{3.73}$$

$$s_{1,h} = s_{0,h} + v_{0,h}t_1 + \frac{1}{2}a_h t_1^2 = s_{0,h} + v_{0,h}t_1 \; (a_h = 0) \tag{3.74}$$

Vertical

$$v_{0,v} = \frac{RPM}{60} 2r_m\pi\sin(\theta_S) \tag{3.75}$$

$$v_{1,v} = 0 = v_{0,v} + a_v t_1 = v_{0v} - gt_1 \tag{3.76}$$

$$s_{0,v} = r_m\sin(\theta_S) \tag{3.77}$$

$$s_{1,v} = s_{0,v} + v_{0,v}t_1 - \frac{1}{2}gt_1^2 \tag{3.78}$$

Solving Equation (3.76) for the upward journey time, t_1,

$$t_1 = \frac{v_{0v}}{g} = \frac{RPM}{60\,g} 2r_m\pi\sin(\theta_S) \tag{3.79}$$

allows the solution of the upward journey system, Equation (3.71) to (3.78).

DOWN

Horizontal

$$v_{1,h} = -\frac{RPM}{60} 2r_m\pi\cos(\theta_S) \tag{3.80}$$

$$v_{2,h} = v_{1,h} \tag{3.81}$$

$$s_{1,h} = s_{0,h} + v_{0,h}t_1 \tag{3.82}$$

$$s_{2,h} = s_{1,h} + v_{1,h}t_2 = s_{0,h} + v_{0,h}(t_1 + t_2) \tag{3.83}$$

Vertical

$$v_{1,v} = 0 \tag{3.84}$$

$$v_{2,v} = v_{1,v} + a_v t_2 \tag{3.85}$$

$$s_{1,v} = s_{0,v} + v_{0,v}t_1 - \frac{1}{2}gt_1^2 \tag{3.86}$$

$$s_{2,v} = s_{1,v} + v_{1,v}t_2 - \frac{1}{2}gt_2^2 = s_{1,v} - \frac{1}{2}gt_2^2 \tag{3.87}$$

$$= s_{0,v} + v_{0,v}t_1 - \frac{1}{2}g(t_1^2 + t_2^2) \tag{3.88}$$

The point of impact (or apparent impact) is at the mill shell, *i.e.*,

$$r_m^2 \quad = \quad s_{2,h}^2 \quad + \quad s_{2,v}^2 \tag{3.89}$$

Inspection of Equations (3.83) and (3.88), reveal that Equation (3.89) is a function of one unknown - t_2 - which may therefore be determined. This allows the solution of the downward journey system, Equation (3.80) to (3.88), and the determination of the impact angle:

$$\theta_I \quad = \quad \arctan\left(\frac{s_{2,v}}{s_{2,h}}\right) \tag{3.90}$$

where

$$\theta_I \quad = \quad \text{angle of ball impact at the mill radius (radians)}$$

When the impact angle is outside the toe angle ($\theta_I \ < \ \theta_T$), impact with the mill shell occurs.

When the impact angle is within or equal to the toe angle ($\theta_I \ \geq \ \theta_T$), impact is at the charge toe or within the boundaries of the charge.

SAG mill model validation

Table 3.4 contains results of the validation of the SAG mill model (in isolation) by way of the stream properties of the rock load and the mill discharge streams. The reference case is the JKSimMet simulation results from the model constructed from the grinding circuit survey (David, 1997), see Appendix B. The feed stream and the columns headed with "JK" is the reference data. The columns headed "model" and "error" are the results from this work and the absolute, relative error between this work and the reference data.

The mill discharge stream shows good agreement with no results further than 3% from the reference case. Although excellent, the agreement in the rock charge results is somewhat misleading. The JKSimMet SAG mill model is intrinsically steady state in nature. The steady state form of Equation (3.1) is solved simultaneously with Equation (3.3) to give a rock load and discharge that satisfies the mass balance. The calculated rock charge is specified as the initial conditions for the rock charge. Since steady state conditions are being simulated, the rock load does not change and thus, agreement is "perfect".

Another SAG mill result of importance is the mill powerdraw. The validation results are in the lower part of Table 3.4 and illustrate good agreement once again.

At this point the SAG mill model was judged valid.

Table 3.4: SAG Mill model validation

Stream Properties	Total Feed	Rock Load			Mill Discharge		
		JK	model	error (%)	JK	model	error (%)
tph_s	252.1	45.7	45.7	0.0	252.1	252.1	0.01
tph_l	80.0	2.1	2.1	0.0	80.0	80.0	0.07
tph_p	332.1	47.7	47.7	0.0	332.1	332.1	0.01
%s w/w	75.9	95.7	95.7	0.0	75.9	75.9	0.02
%l w/w	24.1	4.3	4.3	0.0	24.1	24.1	0.06
m3ph_s	95.1	17.2	17.2	0.0	95.1	95.1	0.01
m3ph_l	80.0	2.1	2.1	0.0	80.0	80.0	0.07
m3ph_p	175.2	19.3	19.3	0.0	175.2	175.1	0.03
%s v/v	54.3	89.3	89.3	0.0	54.3	54.3	0.03
%l v/v	45.7	10.7	10.7	0.0	45.7	45.7	0.04
SGp	2.25	2.58	2.58	0.0	2.25	2.25	0.01
P_{80}	84.0	87.3	87.3	0.0	16.7	16.4	2.0
Powerdraw (kW)		2863	2866	0.1			

3.3.2 Hydrocyclones

The Nageswararao model, which is detailed in Napier-Munn *et al.* (1996), is used to model the primary (and secondary) cyclones. The model is comprised of several equations that are functions of cyclone geometry, feed flowrate and solids density, and, feed ore characteristics.

Cyclone pressure, P, is calculated from the following flowrate equation,

$$Q_f = K_{Q1}D_c{}^2 \left(\frac{P}{\rho_p}\right)^{0.5} \left(\frac{D_o}{D_c}\right)^{0.68} \left(\frac{D_i}{D_c}\right)^{0.45} \theta^{-0.1} \left(\frac{L_c}{D_c}\right)^{0.2} \tag{3.91}$$

where

$$
\begin{aligned}
K_{Q1} &= K_{Q0}D_c^{-0.1} &&\tag{3.92}\\
K_{Q0} &= \text{ore dependent proportionality constant}\\
D_i &= \text{inlet diameter (m)}\\
D_o &= \text{overflow diameter (m)}\\
D_u &= \text{underflow diameter (m)}\\
D_c &= \text{cyclone cylinder diameter (m)}\\
L_c &= \text{cyclone cylinder length (m)}\\
\theta &= \text{cone full angle (}^{\text{o}}\text{)}\\
P &= \text{cyclone inlet pressure (kPa)}\\
\rho_p &= \text{feed pulp (slurry) density (t/m}^3\text{)}\\
Q_f &= \text{cyclone feed flowrate (m}^3\text{/hr)}
\end{aligned}
$$

Cyclone corrected 50% passing size, d_{50c}, is predicted from:

$$\frac{d_{50c}}{D_c} = K_{D1}\left(\frac{D_o}{D_c}\right)^{0.52}\left(\frac{D_u}{D_c}\right)^{-0.47}\lambda^{0.93}\left(\frac{P}{\rho_p g D_c}\right)^{-0.22}\left(\frac{D_i}{D_c}\right)^{-0.5}\left(\frac{L_c}{D_c}\right)^{0.2}\theta^{0.15} \tag{3.93}$$

where

$$
\begin{aligned}
K_{D1} &= K_{D0}D_c^{-0.65} &&\tag{3.94}\\
K_{D0} &= \text{ore dependent proportionality constant}\\
d_{50c} &= \text{corrected 50\% passing size (mm)}\\
g &= \text{gravitational acceleration (9.81 m/s}^2\text{)}
\end{aligned}
$$

The water recovery to cyclone underflow, R_f, is

$$R_f = K_{W1} \left(\frac{D_o}{D_c}\right)^{-1.19} \left(\frac{D_u}{D_c}\right)^{2.40} \left(\frac{P}{\rho_p g D_c}\right)^{-0.53} \lambda^{0.27} \left(\frac{D_i}{D_c}\right)^{-0.50} \theta^{-0.24} \left(\frac{L_c}{D_c}\right)^{0.22} \tag{3.95}$$

where

$$
\begin{aligned}
K_{W1} &= \text{water split to underflow constant} \\
\lambda &= \frac{10^{1.82 C_v}}{(8.05[1 - C_v]^2)} \\
&= \text{hindered settling correction term} \\
C_v &= \text{volumetric fraction of solids in feed slurry (fraction)}
\end{aligned}
\tag{3.96}
$$

The volumetric recovery of feed slurry to cyclone underflow, R_v, is

$$R_v = K_{V1} \left(\frac{D_o}{D_c}\right)^{-0.94} \left(\frac{D_u}{D_c}\right)^{1.83} \left(\frac{P}{\rho_p g D_c}\right)^{-0.31} \left(\frac{D_i}{D_c}\right)^{-0.25} \theta^{-0.24} \left(\frac{L_c}{D_c}\right)^{0.22} \tag{3.97}$$

where

$$K_{V1} \quad = \quad \text{constant to be estimated from data}$$

The size classification function is described by the efficiency to overflow, E_{oa}, equation:

$$E_{oa} = C \left(\frac{(1 + \beta\beta^* x)(e^\alpha - 1)}{e^{\alpha\beta^* x} + e^\alpha - 2}\right) \tag{3.98}$$

where

$$
\begin{aligned}
C &= 1 - R_f \tag{3.99} \\
&= \text{water recovery to cyclone overflow (fraction)} \\
x &= \frac{d}{d_{50c}} \tag{3.100} \\
&= \text{ratio of particle size to corrected 50\% passing size} \\
d &= \text{particle size (mm)} \\
\alpha &= \text{efficiency curve parameter: separation sharpness} \\
\beta &= \text{efficiency curve parameter: fine size efficiency boost} \\
\beta^* &= \text{efficiency curve parameter: } d_{50c} \text{ preservation}
\end{aligned}
$$

The cyclone model calculation sequence is as follows:

1. Given the

   - cyclone dimensions
   - model parameters (α, β, β^*, K_{D0}, K_{Q0}, K_{V1} and K_{W1}) as determined from plant surveys

- feed flowrate and size distribution

2. Calculate cyclone operating pressure from Equation (3.91)

3. Calculate corrected 50% passing size from Equation (3.93)

4. Calculate water recovery to underflow from Equation (3.95)

5. Calculate the separation efficiency to overflow from Equation (3.98)

6. Conduct a mass balance around the cyclone to determine the overflow and underflow streams and size distributions

Cyclone model validation

Table 3.5 contains results of the validation of the primary cyclone model (in isolation) by way of the stream properties of the overflow and underflow streams. The reference case is the JKSimMet simulation results from the model constructed from the grinding circuit survey (David, 1997), see Appendix B. The feed stream and the columns headed with "JK" is the reference data. The columns headed "model" and "error" are the results from this work and the absolute, relative error between this work and the reference data.

Generally, the model results show good agreement with the reference data, with errors of less than 0.2%. The P_{80} result for the overflow stream exhibits a 16% error which is distinctly worse than the other results. This error is attributed to the interpolation method used to arrive at the P_{80} result, $i.e.$, linear interpolation of cumulative weight percent passing $versus$ particle size distribution. The Rosin-Rammler distribution function (Napier-Munn $et\ al.$, 1996) suggests some variation of a log-linear interpolation may be more accurate. However, since the model size distributions were fixed by the points (0.001 mm, 0%passing) and (180.76 mm, 100%passing), a linear extrapolation ($versus$ a smoothing spline extrapolation), of the P_{80} point was utilised for consistency. Good agreement was generally obtained except for the finely-sized streams, such as the cyclone overflows.

Another primary cyclone result of importance is the cyclone operating pressure. The validation results are in the lower part of Table 3.5 and illustrate good agreement once again.

Table 3.5: Primary cyclone model validation

Stream Properties	1° Cyclone Feed	1° Cyclone O/F			1° Cyclone U/F		
		JK	model	error (%)	JK	model	error (%)
tph_s	185.0	34.3	34.3	0.15	150.7	150.7	0.03
tph_l	179.3	117.0	117.0	0.03	62.4	62.3	0.06
tph_p	364.3	151.3	151.3	0.01	213.0	213.0	0.01
%s w/w	50.8	22.7	22.7	0.13	70.7	70.7	0.03
%l w/w	49.2	77.3	77.3	0.04	29.3	29.3	0.06
m3ph_s	69.8	13.0	12.9	0.15	56.9	56.9	0.03
m3ph_l	179.3	117.0	117.0	0.03	62.4	62.3	0.06
m3ph_p	249.1	129.9	129.9	0.01	119.2	119.2	0.01
%s v/v	28.0	10.0	10.0	0.16	47.7	47.7	0.05
%l v/v	72.0	90.0	90.0	0.02	52.3	52.3	0.04
SGp	1.84	1.37	1.37	0.04	2.17	2.17	0.02
P_{80}	2.64	0.06	0.07	15.8	3.24	3.24	0.09
Pressure (kPa)		57.3	57.2	0.17			

Table 3.6: Secondary cyclone model validation

Stream Properties	2° Cyclone Feed	2° Cyclone O/F			2° Cyclone U/F		
		JK	model	error (%)	JK	model	error (%)
tph_s	1099	181.5	181.5	0.0	918	918	0.0
tph_l	564	305	305	0.0	259	259	0.0
tph_p	1663	486	486	0.0	1177	1177	0.0
%s w/w	66.1	37.3	37.3	0.01	78.0	78.0	0.01
%l w/w	33.9	62.7	62.7	0.01	22.0	22.0	0.02
m3ph_s	415	68.5	68.5	0.01	346	346	0.0
m3ph_l	564	305	305	0.01	259	259	0.02
m3ph_p	979	373	373	0.0	605	605	0.01
%s v/v	42.4	18.3	18.3	0.02	57.2	57.2	0.01
%l v/v	57.6	81.7	81.7	0.0	42.8	42.8	0.01
SGp	2.09	1.62	1.62	0.0	2.29	2.29	0.0
P_{80}	0.42	0.09	0.08	6.9	0.50	0.50	0
Pressure (kPa)		150.2	150.2	0.02			

Table 3.6 contains results of the validation of the secondary cyclone model (in isolation) by way of the stream properties of the overflow and underflow streams. The reference case is the JKSimMet simulation results from the model constructed from the grinding circuit survey (David, 1997), see Appendix B. The feed stream and the columns headed with "JK" is the reference data. The columns headed "model" and "error" are the results from this work and the absolute, relative error between this work and the reference data.

Generally, the model results show good agreement with the reference data, with errors of less than 0.02%. As for the primary cyclone overflow, the P_{80} result for the secondary cyclone overflow stream exhibits a larger error ($\approx 7\%$) which is attributed to linear interpolation errors at the fine sizes.

The secondary cyclone operating pressure, in the lower part of Table 3.6, shows good agreement also.

At this point the cyclone model was considered valid.

3.3.3   Oversize Crusher

The model for the oversize crusher is comprised of:

- a particle classification/selection for breakage function

- a breakage distribution function

- a power draw prediction function

Again, it is based on the models developed at the Julius Kruttschnitt Mineral Research Centre, (Whiten, 1972), (Napier-Munn *et al.*, 1996) and (JKTech, 1994).

Crusher Classification Function

The classification function is a selection for breakage function (the Whiten classification model (Napier-Munn *et al.*, 1996)) and provides the probability of breakage *versus* particle size as follows:

$$
\begin{aligned}
C(x) &= 0.0 && \text{for } x < K1 \\
C(x) &= 1.0 - \left(\frac{K2 - x}{K2 - K1} \right)^{K3} && \text{for } K1 \leq x \leq K1 \\
C(x) &= 1.0 && \text{for } x > K2
\end{aligned}
\tag{3.101}
$$

where

$$
\begin{aligned}
C(x) &= \text{probability of breakage (fraction)} \\
K1 &= A_0 \cdot CSS + A_1 \cdot TPH + A_2 \cdot F_{80} + A_3 \cdot LLen + A_4 \tag{3.102} \\
&= \text{particle size below which C(x) = 0 (mm)} \\
K2 &= B_0 \cdot CSS - B_1 \cdot TPH + B_2 \cdot F_{80} + B_3 \cdot LHr + B_4 \cdot ET + B_5 \tag{3.103} \\
&= \text{particle size above which C(x) = 1 (mm)} \\
K3 &= C_0 \text{usually 2.3} \tag{3.104} \\
&= \text{classification function parameter: curve shape}
\end{aligned}
$$

$$
\tag{3.105}
$$

$$
\begin{aligned}
A_i &= \text{model parameters from plant survey} \\
B_i &= \text{model parameters from plant survey} \\
CSS &= \text{crusher close side setting (mm)} \\
TPH &= \text{crusher feedrate (tph)} \\
F_{80} &= \text{crusher feed 80\% passing size (mm)} \\
LLen &= \text{crusher liner length (mm)} \\
LHr &= \text{crusher liner hours in service (hrs)} \\
ET &= \text{crusher eccentric throw (mm)}
\end{aligned}
$$

The oversize crusher probability of breakage function $(C(x))$ is shown in Figure 3.5.
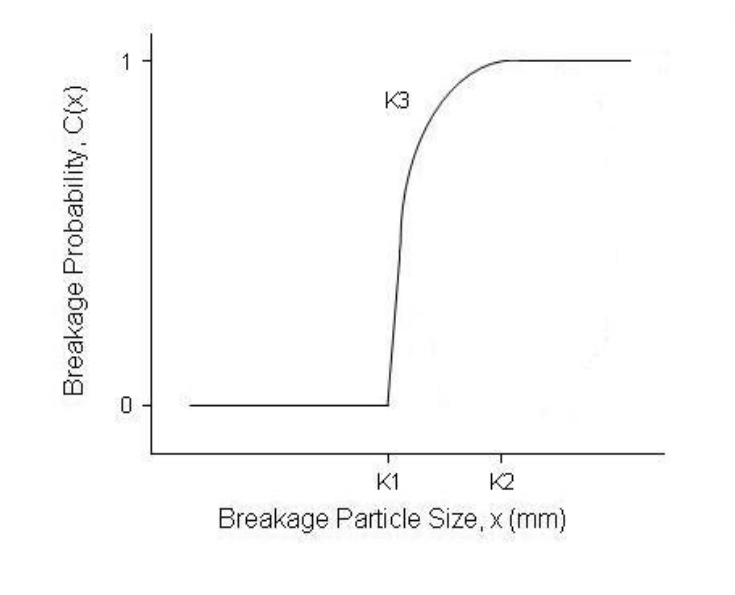

Figure 3.5: Crusher Probability of Breakage Function
(p 141 Napier-Munn et al. (1996))

Breakage Distribution Function

Laboratory ore tests give a crusher breakage parameter, t_{10}, which is a size distribution data identifier, *i.e.*, a look-up table reference point for data in a Julius Kruttschnitt Mineral Research Centre reference database (as described in Section 3.3.1 for the SAG mill appearance function discussion). For the ore in question, the distribution after breakage

is obtained from the database and the fraction of material retained in the size fractions of interest are determined by interpolation. The oversize crusher product is then determined as follows:

$$p \ = \ (1 - C) \cdot (1 - BC)^{-1} \cdot f \qquad (3.106)$$

where

$$p \ = \ \text{crusher product by size (tph)}$$

$$f \ = \ \text{crusher feed by size (tph)}$$

$$B \ = \ \text{crusher breakage distribution function (fraction)}$$

$$C \ = \ = \text{C(x)} = \text{crusher probability of breakage function (fraction)}$$

Equation (3.106) is the crusher mass balance equation which is implicitly steady state, *i.e.*,

- no accumulation (feed tph = product tph)

- any water in the feed reports to product

Crusher Power draw Prediction

The oversize crusher power draw is determined as follows:

1. for the ore specific crusher t_{10} parameter, the specific comminution energy, *Ecs* (kWh/t), *versus size* relationship is determined by interpolation against a Julius Kruttschnitt Mineral Research Centre database

2. the *Ecs* for the size fractions of interest are determined by interpolation against the result from Step 1.

3. the pendulum power, P_p, is determined by Equation (3.107)

4. predicted crusher power draw, P_c, is then determined by Equation (3.108)

$$P_p = \sum Ecs_i C_i f_i \tag{3.107}$$

$$P_c = A P_p + P_n \tag{3.108}$$

where

$$
\begin{aligned}
P_p &= \text{pendulum power (kW)} \\
P_c &= \text{predicted crusher power draw (kW)} \\
P_n &= \text{crusher no-load power (kW)} \\
Ecs_i &= \text{specific comminution energy by size (kWh/t)} \\
C_i &= \text{crusher probability of breakage function (fraction)} \\
f_i &= \text{crusher feedrate by size (tph)} \\
A &= \text{dimensionless scaling factor}
\end{aligned}
$$

Oversize crusher model validation

Table 3.7 contains results of the validation of the oversize crusher model (in isolation) by way of the stream properties of the crusher product stream. The reference case is the JKSimMet simulation results from the model constructed from the grinding circuit survey (David, 1997), see Appendix B. The feed stream and the columns headed with "JK" is the reference data. The columns headed "model" and "error" are the results from this work and the absolute, relative error between this work and the reference data.

Generally, the model results show excellent agreement with the reference data. As for the cyclone overflow streams, the P_{80} result for the crusher product stream exhibits a larger error (12%) which is attributed to linear interpolation errors at the fine sizes.

The crusher powerdraw, in the lower part of Table 3.7, shows good agreement also.

At this point the oversize crusher model was judged valid.

Table 3.7: O/S Crusher model validation

Stream Properties	O/S Crusher Feed	O/S Crusher Product		
		JK	model	error (%)
tph_s	67.1	67.1	67.1	0
tph_l	0.05	0.05	0.05	0
tph_p	67.1	67.1	67.1	0
%s w/w	99.9	99.9	99.9	0
%l w/w	0.1	0.1	0.1	0
m3ph_s	25.3	25.3	25.3	0
m3ph_l	0.05	0.05	0.05	0
m3ph_p	25.4	25.4	25.4	0
%s v/v	99.8	99.8	99.8	0
%l v/v	0.2	0.2	0.2	0
SGp	2.65	2.65	2.65	0
P_{80}	42.9	34.0	37.9	11.5
Powerdraw (kW)		42.8	41.9	1.9

3.3.4 Mill Discharge Screens

The mill discharge screens are modelled as a simple efficiency curve, similar to the efficiency to overflow, E_{oa}, curve used for the primary cyclones, see Equation (3.98). The corrected 50% passing size, d_{50c}, and water recovery to underflow, R_f, are calculated in the case of the cyclone model. However, in the discharge screen model these two parameters are specified (as determined from surveyed screen performance).

Screen model validation

Table 3.8 contains results of the validation of the SAG mill discharge screen model (in isolation) by way of the stream properties of the oversize and undersize streams. The reference case is the JKSimMet simulation results from the model constructed from the grinding circuit survey (David, 1997), see Appendix B. The feed stream and the columns headed with "JK" is the reference data. The columns headed "model" and "error" are the results from this work and the absolute, relative error between this work and the reference data.

Generally, the model results show good agreement with the reference data, with errors of less than 0.3%, including the P_{80} results. The largest errors occur in the water balance ($\approx 6\%$). This is due to the screen oversize being virtually dry. Small errors in the water content of the stream translate to larger relative errors.

Table 3.9 contains results of the validation of the ball mill discharge screen model (in isolation) by way of the stream properties of the oversize and undersize streams. The reference case is the JKSimMet simulation results from the model constructed from the grinding circuit survey (David, 1997), see Appendix B. The feed stream and the columns headed with "JK" is the reference data. The columns headed "model" and "error" are the results from this work and the absolute, relative error between this work and the reference data.

Generally, the model results show good agreement with the reference data, with errors of less than 0.1%. The largest error, $\approx 2\%$, is in screen oversize P_{80} estimate.

At this point the screen model was considered valid.

Table 3.8: SAG mill discharge screen model validation

Stream Properties	SAG mill Screen feed	Screen Oversize			Screen Undersize		
		JK	model	error (%)	JK	model	error (%)
tph_s	252.1	67.1	67.1	0.03	185.0	185.0	0.01
tph_l	94.9	0.05	0.06	6.15	95.0	94.9	0.06
tph_p	347.0	67.1	67.1	0.02	280.0	279.9	0.01
%s w/w	72.6	99.9	99.9	0.0	66.1	66.1	0.02
%l w/w	27.4	0.1	0.1	6.1	33.9	33.9	0.05
m3ph_s	95.1	25.3	25.3	0.03	69.8	69.8	0.01
m3ph_l	94.9	0.05	0.06	6.1	95.0	94.9	0.06
m3ph_p	190.1	25.4	25.4	0.01	164.8	164.7	0.03
%s v/v	50.0	99.8	99.8	0.01	42.4	42.4	0.04
%l v/v	50.0	0.2	0.2	6.1	57.6	57.6	0.03
SGp	2.20	2.65	2.65	0.0	2.09	2.09	0.01
P_{80}	16.7	42.9	42.9	0.05	2.64	2.65	0.20

Table 3.9: Ball mill discharge screen model validation

Stream Properties	Ball mill Screen feed	Screen Oversize			Screen Undersize		
		JK	model	error (%)	JK	model	error (%)
tph_s	1068	3.4	3.4	0.1	1065	1065	0.0
tph_l	336	0.0	0.0	0.0	336	336	0.0
tph_p	1405	3.4	3.4	0.1	1401	1401	0.0
%s w/w	76.1	99.3	99.3	0.0	76.0	76.0	0.0
%l w/w	23.9	0.7	0.7	0.09	24.0	24.0	0.01
m3ph_s	403	1.3	1.3	0.06	402	402	0.0
m3ph_l	336	0.02	0.02	0.0	336	336	0.01
m3ph_p	739	1.3	1.3	0.07	738	738	0.01
%s v/v	54.5	98.2	98.2	0.0	54.5	54.5	0.0
%l v/v	45.5	1.8	1.8	0.08	45.5	45.5	0.0
SGp	2.26	2.64	2.64	0.0	2.25	2.25	0.0
P_{80}	0.44	11.6	11.3	2.3	0.43	0.43	0.05

3.3.5   Ball Mill

The ball mill model is similar to the SAG mill model, described in Section 3.3.1, and consists of:

- solids balance
- water balance
- ball charge model
- power draw model

Mass Balances

Water :   The steady state water balance for the ball mill is simply

$$Water\ In\ =\ Water\ Out \tag{3.109}$$

Solids :   The steady state solids mass balance for the ball mill (Valery Jnr and Morrell, 1995) and (Napier-Munn *et al.*, 1996) is:

$$
\begin{aligned}
0 &= \text{In - Out + Generation - Consumption} \\
0 &= f_i - p_i + \sum_{j=1}^{i-1} r_j s_j a_{ij} - (1 - a_{ii}) r_i s_i
\end{aligned}
\tag{3.110}
$$

where
$$
\begin{aligned}
s_i &= \text{mill rock charge particles in } size i \text{ (t)} \\
f_i &= \text{feedrate of particles in } size\ i \text{ (t)} \\
p_i &= \text{mill discharge (product) of particles in } size\ i \text{ (t)} \\
r_i &= \text{breakage rate of particles in } size\ i \text{ (hr}^{-1}) \\
a_{ij} &= \text{appearance function of particles appearing in } size\ i \text{ (a func-} \\
&\quad \text{tion of the breakage distribution of particles in sizes} \geq size\ i) \\
&\quad \text{(fraction)}
\end{aligned}
$$

The feed component in Equation (3.110) is obtained by the summation of the:

- primary cyclone underflow to the ball milll,
- secondary cyclone underflow to the ball mill, and,
- the flash flotation tails stream.

The ball mill product, generation and consumption components are dealt with differently to the SAG mill. These terms will now be discussed further.

Product

The ball mill product, p_i, (the ball mill discharge stream, $BMDC$) is calculated as follows:

$$p_i \;=\; d_i s_i \tag{3.111}$$

where

$$d_i \;=\; d_i^* \left(\frac{4Q}{D_m^2 L_m} \right) \;=\; d_i^* \frac{1}{\tau} \tag{3.112}$$

$$\;=\; \text{mill discharge rate of } size\ i \text{ particles (hr}^{-1})$$

$$d_i^* \;=\; \text{mill discharge rate of } size\ i \text{ particles normalised to mill residence time } (-)$$

$$\frac{D_m^2 L_m}{4Q} \;=\; \tau = \text{mill residence time (hr)} \tag{3.113}$$

$$\frac{1}{\tau} \;=\; \text{mill space velocity (hr}^{-1}) \tag{3.114}$$

$$D_m \;=\; \text{mill inside diameter (m)}$$

$$L_m \;=\; \text{mill length (m)}$$

Rearranging Equation (3.111) for s_i and substituting into Equation (3.110) yields Equation (3.115) which can be solved for mill product, p_i, once the appearance function, a_{ij}, and the rate/discharge function, $\frac{r_i}{d_i^*}$, have been specified.

$$0 \;=\; f_i \;-\; p_i \;+\; \tau \sum_{j=1}^{i-1} \frac{r_j}{d_j^*} p_j a_{ij} \;-\; (1 - a_{ii})\tau \frac{r_i}{d_i^*} p_i \tag{3.115}$$

where

$$\frac{r_i}{d_i^*} \;=\; \text{ball mill rate/discharge value for } size\ i \text{ particles (hr}^{-1})$$

Generation and Consumption

As mentioned above, the ball mill appearance function, a_{ij}, and the rate/discharge function, $\frac{r_i}{d_i^*}$ function are specified in the ball mill model and are determined by laboratory scale ore ball milling tests.

Appearance Function, a_{ij} :   Similar to the the SAG mill appearance function, the ball mill appearance function is a matrix of vectors that describe:

1. the amount of material in a given size that is "selected" for breakage, and,

2. the distribution that remains after breakage has occurred

Similar to the SAG mill appearance function matrix, the ball mill appearance function matrix is a square matrix of size (no. of sizes × no. of sizes). Also, since there is no particle growth, the appearance function matrix is a lower-triangular matrix. Unlike the SAG mill, the appearance vector is the same for each particle size. This is a result of type of breakage occurring in the mill. Only abrasion (low energy) breakage occurs in a ball mill and the resulting breakage distribution is independent of size.

Rate/Discharge Function, $\frac{r_i}{d_i^*}$:   The rate/discharge function is determined from data obtained during plant surveys and by a model fitting process. The full function for a given ball mill is condensed to a set of four (4) ("knot size", $ln(\frac{r}{d^*})$) pairs. The knot sizes are selected to encompass the size distribution and capture important features,such as the maximum breakage rates of intermediately sized particles. The rate/discharge values for each particle size is determined by interpolation.

Ball Charge Model

The ball mill ball charge model simply consists of:

1. a specified ball charge level, J_b

2. a specified ball top size (in mm)

Both of these parameters are specified by plant survey data.

Model Scaling

To increase the utility of the ball mill model, a number of scaling factors are used to adjust the rate/discharge function values according to the prevailing operating conditions (*wrt*

the conditions for which the original model was developed), see Equation (3.116).

$$
\frac{\left(\frac{r}{d^*}\right)_{SIM}}{\left(\frac{r}{d^*}\right)_{FIT}} = \left(\frac{D_{SIM}}{D_{FIT}}\right)^{0.5} \left(\frac{1 - LF_{SIM}}{1 - LF_{FIT}}\right) \left(\frac{LF_{SIM}}{LF_{FIT}}\right) \left(\frac{C_{s\,SIM}}{C_{s\,FIT}}\right) \left(\frac{WI_{SIM}}{WI_{FIT}}\right)^{0.8} \quad (3.116)
$$

where

$$
\begin{aligned}
D &= \text{mill inside diameter (m)} \\
LF &= J_b = \text{ball charge fraction } (J_b) \text{ (fraction)} \\
C_s &= \frac{42.3}{\sqrt{D}} = \text{mill critical speed (RPM)} \quad (3.117) \\
WI &= \text{ore work index (kWh/t)} \\
_{FIT} &= \text{original conditions of fitted model} \\
_{SIM} &= \text{simulated conditions}
\end{aligned}
$$

Model scaling on account of ball size is divided around size x_m, the size below which, abrasion breakage predominates and above which, impact breakage predominates, see Equation (3.118).

$$
x_m = K \cdot b^2 \quad (3.118)
$$

where

$$
\begin{aligned}
K &= \text{maximum breakage factor (mm}^{-1}) \\
b &= \text{ball diameter (mm)} \\
x_m &= \text{impact } versus \text{ abrasion breakage boundary particle size (mm)}
\end{aligned}
$$

For particle sizes, $x \leq x_m$,

$$
\frac{\left(\frac{r}{d^*}\right)_{SIM}}{\left(\frac{r}{d^*}\right)_{FIT}} = \frac{b_{FIT}}{b_{SIM}} \quad (3.119)
$$

For particle sizes, $x > x_m$,

$$
\frac{\left(\frac{r}{d^*}\right)_{SIM}}{\left(\frac{r}{d^*}\right)_{FIT}} = \left(\frac{b_{SIM}}{b_{FIT}}\right)^2 \quad (3.120)
$$

Power draw Model

The ball mill power draw model is the same as that detailed for SAG mill power draw in Section 3.3.1.

Ball mill model validation

Table 3.10 contains results of the validation of the ball mill model (in isolation) by way of the stream properties of the ball mill discharge stream. The reference case is the JKSimMet simulation results from the model constructed from the grinding circuit survey (David, 1997), see Appendix B. The feed stream and the columns headed with "JK" is the reference data. The columns headed "model" and "error" are the results from this work and the absolute, relative error between this work and the reference data.

Generally, the model results show excellent agreement with the reference data with all errors less than 0.6%. The reference data lacked a ball mill powerdraw figure. The ball mill is rated to 3000 kW. The model power parameter, k, can be adjusted so that the agreement is better than the tabulated 5%. Therefore this aspect of the model is considered valid also.

At this point the ball mill model was judged valid.

Table 3.10: Ball mill model validation

Stream	Ball mill	O/S Ball mill discharge		
Properties	Feed	JK	model	error (%)
tph_s	1069	1068	1069	0.0
tph_l	321	321	321	0.0
tph_p	1390	1390	13890	0.0
%s w/w	76.9	76.9	76.9	0.01
%l w/w	23.1	23.1	23.1	0.02
m3ph_s	403	403	403	0.01
m3ph_l	321	321	321	0.03
m3ph_p	724	724	724	0.02
%s v/v	55.7	55.7	55.7	0.01
%l v/v	44.3	44.3	44.3	0.01
SGp	2.27	2.27	2.27	0.0
P_{80}	0.64	0.44	0.44	0.5
Powerdraw (kW)		≈ 3000	3148	4.9

3.3.6 Flash Flotation Cells

At the time of the grinding circuit surveys (early 1997) the flash flotation cells were either being installed or commissioned. As a result, the flash flotation cells were not in operation during the surveys. Furthermore, a detailed model was not developed for the NPM flash flotation cells by the JKTech personnel. Therefore, to achieve a full circuit model, a simplified model would need to be utilised for the flash flotation cells. The model proposed for such utilisation is a simple efficiency curve, similar to that utilised for the SAG mill discharge screen, see Section 3.3.4. Again, the corrected 50% passing size, d_{50c}, and water recovery to underflow (tails), R_f, are specified model parameters (that would have to be determined by plant survey).

In the absence of operating data, or, a reference JKSimMet simulation case, validation of a flash flotation model is not feasible. Therefore, the flash flotation cells have been omitted from the full circuit model.

3.4 Steady State Circuit Model Validation

Once the individual equipment models were constructed and validated they were joined together to form the full circuit as per the grinding circuit survey (David, 1997). Operating conditions characteristic of the survey are:

- zero recycle of primary cyclone underflow to the SAG mill

- flash flotation cells not operating

Table 3.11 through Table 3.14 show the comparative error between the model simulation results and the base case data (David, 1997), see Appendix B. For brevity, comparative Stream Properties results only are shown here. Appendix C contains the reference data and the simulation results in full. The Appendix B survey data was simulated on a unit by unit basis by the MATLAB-Simulink models to produce the reference data in Appendix C. Table C.1 through Table C.4 contains the stream properties and size distribution information for the reference data. Table C.5 through Table C.8 contains the stream properties and size distribution information for the full circuit MATLAB-Simulink simulation model results. The size distribution information for these two cases (and the inferential model case) are shown graphically in Figure C.1 through Figure C.8[8].

Referring again to Tables 3.11 to 3.14, the agreement is generally acceptable with many of the results exhibiting errors of $< 1\%$. There are a number of results which exhibit errors significantly larger and these will now be addressed in more detail.

Table 3.11 contains the results for the "front-end" of the primary grinding circuit and Table 3.12 contains the results for the "back-end" of the primary grinding circuit. Again, agreement is generally acceptable at $< 1\%$. It should be noted that the SAG mill fresh feed and rock charge, $SMFF$ & $SMRC$, respectively, are specified information. Further details are as follows:

- The oversize crusher feed ($OSCF$) and product ($OSCP$) exhibit $\approx 6\%$ error in the water flow. These are essentially dry streams. Therefore, small differences in water flowrates correspond to larger relative errors.

- The SAG mill and oversize crusher powerdraw and the primary cyclone pressure estimates exhibit good agreement.

- A number of the eighty percent passing size (P_{80}) results show significant deviation from the base case information. These deviations are attributed to interpolation errors combined with minor model approximations. The commercial simulation package (JKSimMet) utilises splines to describe size distributions and for interpolation. Linear description and interpolation (fixed by the points (0.001 mm, 0%passing) and (180.76 mm, 100%passing)) are considered sufficiently accurate in this research and thus are utilised in the MATLAB-Simulink models.

Furthermore, for fine streams, such as the primary cyclone overflow ($PCOF$) and underflow ($PCUF$), where the reference data is of the order of 10^1 to $10^3\,\mu$m, small differences between simulation and reference data are simply relatively larger.

The P_{80} measure is also an attempt at a single point measure of a full size distribution. Relative movement in the P_{80} measurement over time is the most important consideration rather than the absolute value of the measurement itself (Davies *et al.*, 2000) .

The difference in interpolation methods is one of the minor model approximations. Manual fitting of model parameters was utilised predominantly in the model development phase. In the JKSimMet software, model fitting, using least squares minimisation techniques, is conducted prior to conducting simulations. Manual model parameter fitting was considered sufficiently accurate in this research and proved insightful regarding model sensitivity.

Considering these points, the simulation results, including the P_{80} results, are considered acceptable.

Table 3.13 contains the results for the "front-end" of the secondary grinding circuit and Table 3.14 contains the results for the "back-end" of the secondary grinding circuit. Here the level of agreement is lower than the for the primary circuit and there is also a wider range in the results. These features are due to the propagation of errors from upstream information combined with model parameter influences. Certain parameters were selected to achieve close agreement for the grinding circuit product stream (secondary cyclone overflow, $SCOF$) at the expense of lower agreement levels for some streams internal to the circuit,*e.g.*, secondary cyclone underflow, $SCUF$. Further points of discussion are:

- The P_{80} remarks above regarding interpolation methods and model approximations apply here also.

- The "dry stream" comments above apply for the ball mill screen oversize ($BSOS$) here.

- Water results throughout the secondary survey are strongly influenced by the circulating water in the secondary cyclone underflow ($SCUF$) stream which is a result of model parameter influences mentioned above.

- Ball mill powerdraw and secondary cyclone pressure estimates display good agreement.

In conclusion, these results (Table 3.11 through Table 3.14) and those in Appendix C display satisfactory agreement with the reference data outright, especially once the propagation of errors and the influence of model parameters have been considered. Therefore, at this point the steady state grinding circuit model is deemed valid.

Table 3.11: Simulation Errors: Primary Circuit - SAG mill

Stream Properties	SMFF	OSCP	SMTF	SMRC	SMDC
tph_s	0.0	0.1	0.0	0.0	0.0
tph_l	0.0	6.0	0.0	0.0	0.1
tph_p	0.0	0.1	0.0	0.0	0.0
%s w/w	0.0	0.0	0.0	0.0	0.0
%l w/w	0.0	5.9	0.0	0.0	0.1
m3ph_s	0.0	0.1	0.0	0.0	0.0
m3ph_l	0.0	6.0	0.0	0.0	0.1
m3ph_p	0.0	0.1	0.0	0.0	0.0
%s v/v	0.0	0.0	0.0	0.0	0.0
%l v/v	0.0	5.9	0.0	0.0	0.0
SGp	0.0	0.0	0.0	0.0	0.0
P_{80}	0.0	20.0	0.0	0.0	2.0
Power				2.2	
Pressure					

Table 3.12: Simulation Errors: Primary Circuit - Screen/Crusher/Cyclones

Stream Properties	SMDC	OSCF	OSCP	PCFD	PCUF	PCOF
tph_s	0.0	0.1	0.1	0.0	0.0	0.1
tph_l	0.1	6.0	6.0	0.1	0.0	0.1
tph_p	0.0	0.1	0.1	0.0	0.0	0.1
%s w/w	0.0	0.0	0.0	0.0	0.0	0.0
%l w/w	0.1	5.9	5.9	0.0	0.0	0.01
m3ph_s	0.0	0.1	0.1	0.0	0.0	0.1
m3ph_l	0.1	6.0	6.0	0.1	0.0	0.1
m3ph_p	0.0	0.1	0.1	0.1	0.0	0.1
%s v/v	0.0	0.0	0.0	0.0	0.0	0.0
%l v/v	0.0	5.9	5.9	0.0	0.0	0.0
SGp	0.0	0.0	0.0	0.0	0.0	0.0
P_{80}	2.0	34	20	95	90	36
Power			5.2			
Pressure				0.3		

Table 3.13: Simulation Errors: Secondary Circuit - Ball mill/Screen

Stream Properties	PCUF	SCUF	BMFD	BMDC	BSOS	BSUS
tph_s	0.0	0.1	0.1	0.1	3.8	0.1
tph_l	0.0	45	36	36	34	34
tph_p	0.0	9.9	8.	8.4	3.6	8.3
%s w/w	0.0	8.9	7.7	7.7	0.3	7.6
%l w/w	0.0	32	25	26	39	24
m3ph_s	0.0	0.1	0.1	0.1	3.8	0.1
m3ph_l	0.0	45	36	36	34	34
m3ph_p	0.0	19	16	16	3.1249	16
%s v/v	0.0	16.0	13.7	13.7	0.7	13.5
%l v/v	0.0	21.4	17.2	17.3	39	16.2
SGp	0.0	0.1	0.1	0.1	0.1	0.1
P_{80}	90	41	38	34	48	33
Power						
Pressure				≤ 10		

Table 3.14: Simulation Errors: Secondary Circuit - Cyclones

Stream Properties	BSUS	PCOF	SCFD	SCUF	SCOF
tph_s	0.1	0.1	0.1	0.1	0.0
tph_l	34	0.1	20.5	45	0.0
tph_p	8.4	0.1	7.0	9.9	0.0
%s w/w	7.6	0.0	6.5	8.9	0.1
%l w/w	24.1	0.0	12.6	32	0.
m3ph_s	0.1	0.1	0.1	0.1	0.0
m3ph_l	34	0.1	20.5	45	0.1
m3ph_p	15.7	0.1	11.9	19.2	0.0
%s v/v	13.5	0.0	10.5	16.0	0.1
%l v/v	16.1	0.0	7.7	21.4	0.0
SGp	0.1	0.0	0.1	0.1	0.0
P_{80}	33	36	32	41	49
Power					
Pressure			0.1		

3.5   Supplementary Model Validation: Gault Data

3.5.1   Process Description

The steady state models discussed above were further validated against data published in a University of Queensland PhD Thesis, (Gault, 1975). The results of the base case of the Kambalda Nickel Operation (KNO) rock-pebble mill circuit, shown in Figure 3.6, were selected as reference for further model validation.

The fresh ore (-9.5 mm) is fed to a rock mill, which is periodically charged with rock media ($+127$ to -203 mm). Rock mill discharge is presented to a DSM sieve bend, which recycles screen oversize to the rock mill and feeds screen undersize to a Krebs D20B cyclone[3]. Cyclone overflow represents the circuit product, which reports to the flotation plant. Cyclone underflow is fed to a pebble mill, which is periodically charged with pebble media ($+76$ to -127 mm). Pebble mill discharge joins the rock mill discharge stream reporting to the DSM sieve bend. Table 3.15 contains the key details of the processing units within the KNO circuit and the modelling parameters utilised. The DSM Screen was modelled as an efficiency curve.
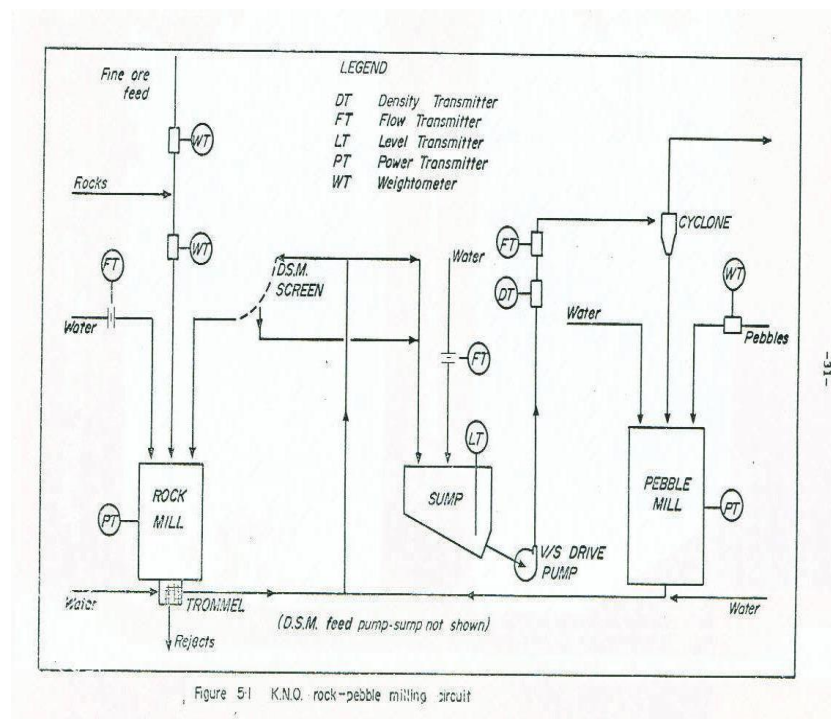
Figure 3.6: KNO Grinding Circuit

---

[3]Cyclone dimensions taken from the supplementary information manual of the *JKSimMet* Manual (JKTech, 1994)

The SAG mill model requires numerous parameters, such as ore hardness and breakage parameters (A, b and ta), an initial estimate of the SAG mill rock charge, discharge grate characteristics (fractional grate open area, relative open area of the pebble ports, relative radial position of open area and relative radial position of outer grate) and numerous others. These parameters were not presented by Gault (1975), presumably because the SAG model was not at its current stage of development. Educated guess-work could be used to estimate a number of the parameters. However, determination of all of the required parameters and the full definition of the SAG mill model is not possible. Therefore, the SAG mill was modelled as a ball mill to fulfill the objective of obtaining a full circuit model.

A major consequence of this simplification was that simulation of the dynamic tests conducted by Gault (1975) were not possible to replicate. However, this unfortunate development did not compromise the model validation objective. The results presented below reinforce the validation of the steady state models. Regarding the further validation of the inferential measurement models developed in Chapter 5, fortuitously, Northparkes Mines data was sourced from the time of the *SAG Control Project* (Romagnoli *et al.*, 1997) , which was able to be utilised for this purpose. Section 8.1 details this further validation of the inferential models.

3.5.2   Validation Results

Figure 3.7 shows the simulation model Rock Mill discharge presented alongside the KNO Rock Mill discharge. Visual inspection shows a good match between the simulation results and the Gault reference data. These results reinforce the validity of the simulation models utilised in this research, especially considering minimal, manual model fitting was conducted. The in-built model-fitting functionality of *JKSimMet* is not a feature of the models utilised in this research. The latter two points apply throughout the following discussion.

The Pebble Mill discharge results are shown in Figure 3.8. The close fit of the Rock Mill discharge is not evident here. However, the fit between the simulation model and the Gault data was considered satisfactory, which reinforced the validity of the ball mill model utilised in this research.

Table 3.15: KNO Process Units

Unit	Dimensions
Rock Mill	Mill Diameter, $D_{mill} = 3.20$ m
	Mill Length, $L_{mill} = 4.10$ m
	Frac. Critical Speed, $N_{fcs} = 78$ %
	Cone Angle, $\theta = 15$ ^{o}
	Trunnion Diameter, $D_t = 0.75$ m
Trommel Screen	Aperture = 7.9 mm
DSM Screen	Aperture = 5 mm
Pebble Mill	Mill Diameter, $D_{mill} = 3.81$ m
	Mill Length, $L_{mill} = 5.79$ m
	Frac. Critical Speed, $N_{fcs} = 67$ %
	Cone Angle, $\theta = 15$ ^{o}
	Trunnion Diameter, $D_t = 0.75$ m
Cyclone	Krebs D20B
	Cyclone Diameter, $D_c = 0.508$ m
	Inlet Diameter, $D_i = 0.157$ m
	Outlet Diameter, $D_o = 0.203$ m
	Underflow Diameter, $D_u = 0.152$ m
	Cylinder Length, $L_c = 0.32$ m
	Cone Angle, $\theta = 20$ ^{o}

Figures 3.9, 3.10 and 3.11 illustrate the simulation model results *versus* the Gault data for the DSM sieve bend, Rock Mill trommel screen and cyclone, respectively. The DSM sieve bend results, Figure 3.9, are mixed. There is excellent agreement for the fine undersize stream, while there is a lesser degree of agreement for the coarse oversize stream. This latter diversion is attributed to the low degree of separation effected by the DSM sieve bend.
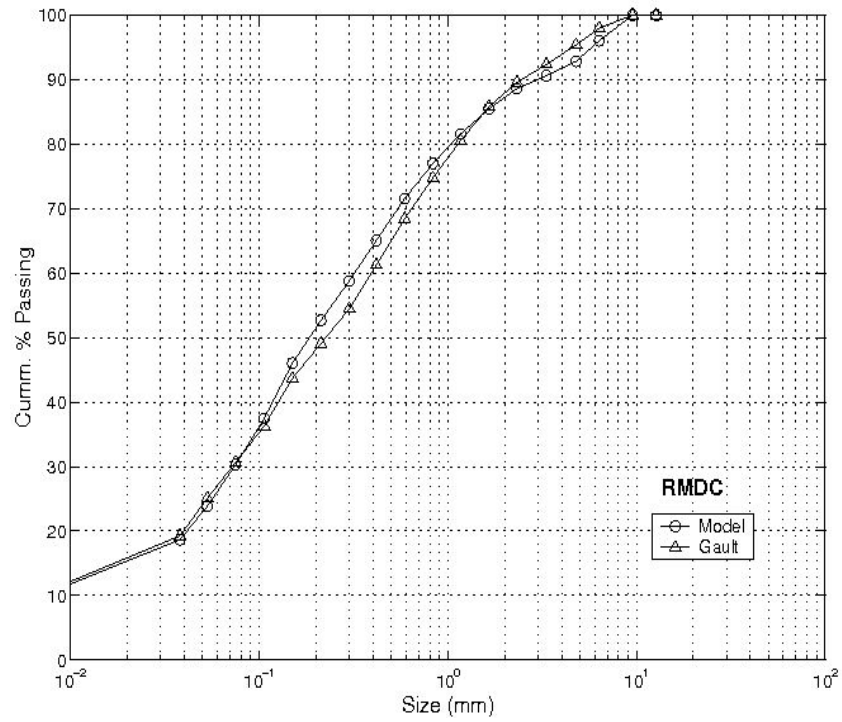
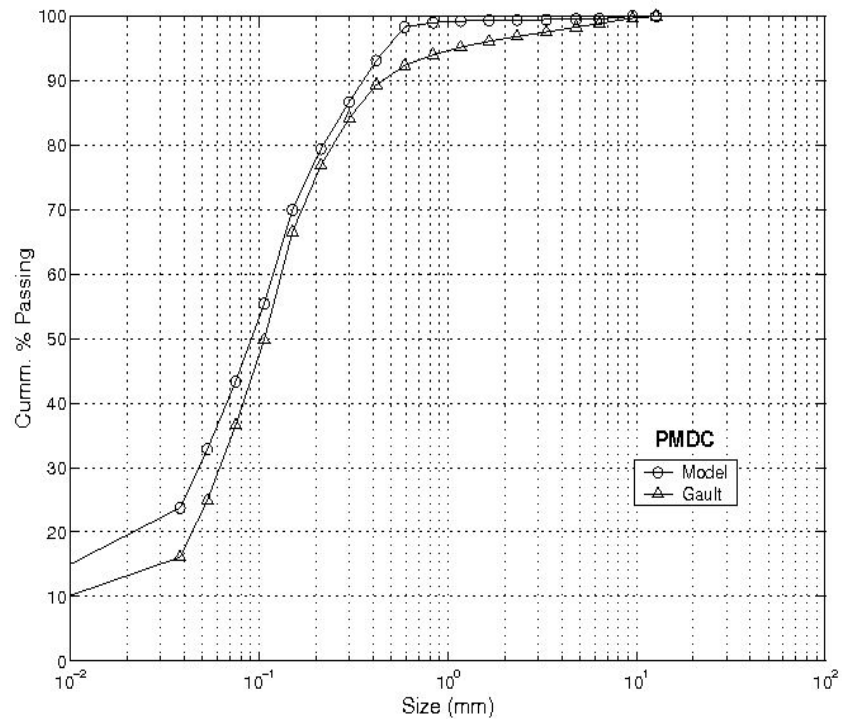Figure 3.7: KNO Rock Mill Discharge

Figure 3.8: KNO Pebble Mill Discharge

The undersize stream distribution is similar to the feed distribution. Small modelling inaccuracies are emphasized in the stream that is extracted from the bulk material, the coarse stream in this instance. The model fitting effort was limited by time constraints. Furthermore, the relative, perceived insignificance of supplementary model validation of a DSM sieve bend curtailed further model fitting. The results for the DSM sieve bend as they stand, and considering the latter points, are considered sufficient to deem the sieve bend model valid.

The Rock Mill trommel screen results are shown in Figure 3.10. There is good agreement at the top and bottom of the distribution. There is lesser agreement mid-distribution. The discrepancies in the results are attributed to the sharp separation required to model the narrow trommel oversize distribution. Such a sharp separation requires thorough model-fitting, which was not afforded to this problem on account of time constraints and the relative insignificance of the trommel screen modelling task. The results were considered sufficiently satisfactory and the trommel screen model, therefore, was considered valid.

Figure 3.11 illustrates the cyclone stream results. There is a relatively low degree of separation occurring at the cyclone, with the cyclone underflow being not altogether dissimilar to the cyclone feed. This is a contributing factor to the errors evident in the results. Other contributing factors are related to the cyclone dimensions and the cyclone modelling parameters.

The cyclone is a *Krebs D20B* cyclone, the dimensions or which are not detailed by Gault (1975). The dimensions listed in Table 3.15 were sourced, as previously mentioned, from the supplementary information booklet of the *JKSimMet* Manual (JKTech, 1994). There is no way to ascertain the applicability of these dimensions to the KNO cyclone.

The Nageswararao cyclone model, detailed in Napier-Munn *et al.* (1996) and utilised in this research relies on numerous cyclone dimension, ore property and efficiency curve parameters. As mentioned, the cyclone dimensions utlised contain a degree on uncertainty. Best estimates of the ore-property parameters were sourced from the supplementary information booklet of the *JKSimMet* Manual (JKTech, 1994). Time constraints and research focus curtailed the model-fitting effort. Considering these points, the model-fit achieved was considered sufficient to prove the validity of the cyclone models utilised in this research.
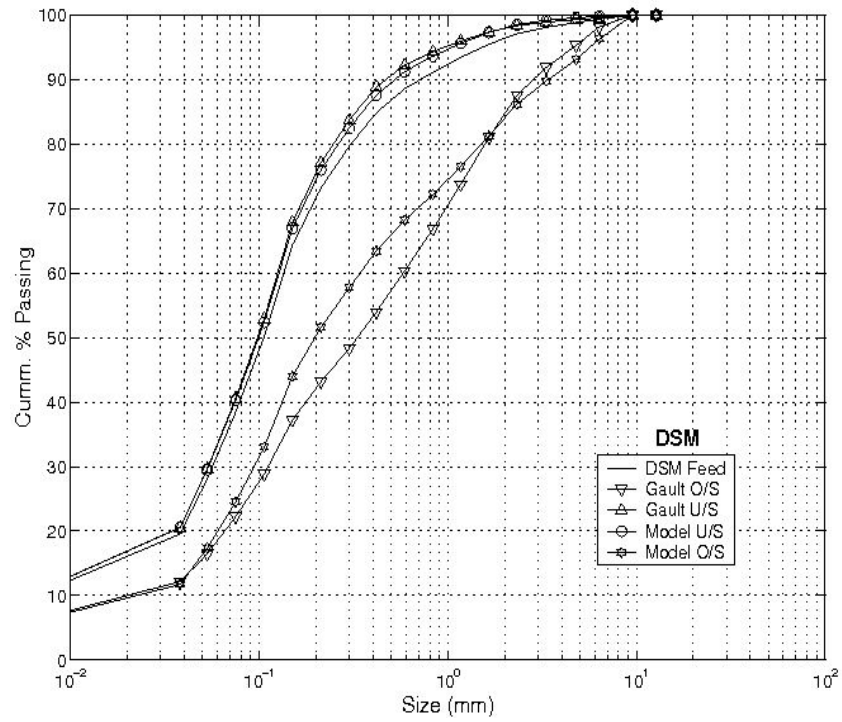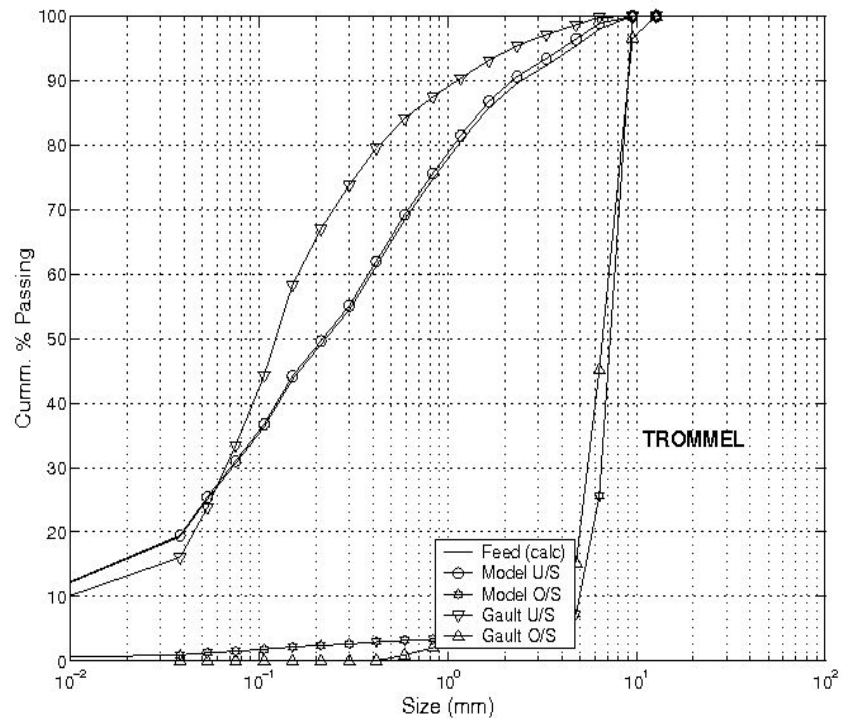
Figure 3.9: KNO DSM Screen Streams
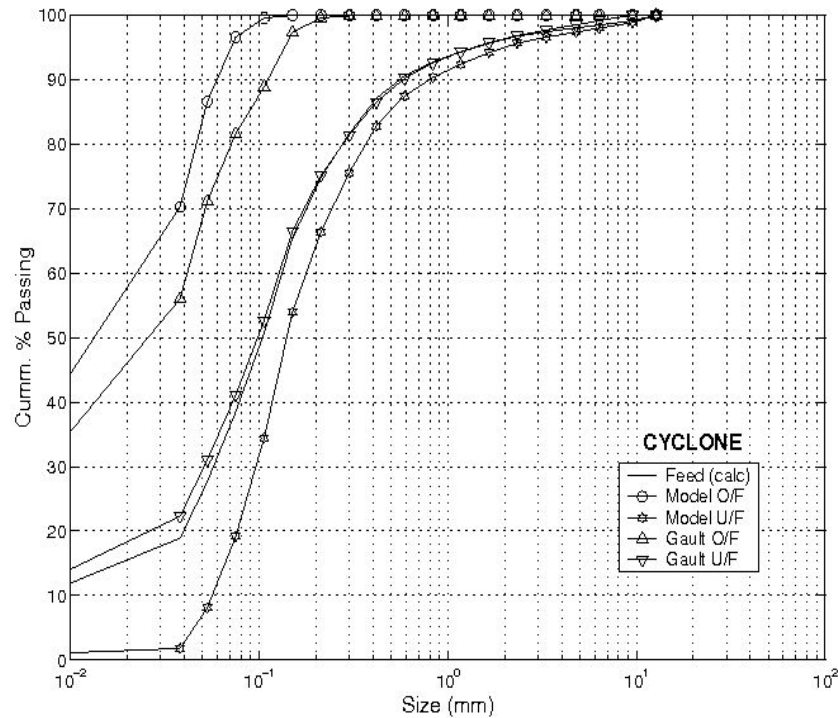

Figure 3.10: KNO Trommel Screen Streams

Figure 3.11: KNO Cyclone Streams

In conclusion, the supplementary model validation, based on the data published in Gault (1975) and presented in summary by way of Figures 3.7 through 3.11, reinforce the conclusions of Sections 3.3 and 3.4 that the steady state unit process models and the steady state grinding circuit model are valid.

The model validation conducted in this Chapter has been the comparison of the MATLAB-Simulink model results to the results generated by JKSimMet (the commercially available software) for the same circuit. This degree of validation was dictated by access to the process and the independent nature of this research, *i.e.*, comminution research without the support of a comminution research resource-base, such as the Julius Kruttschnitt Mineral Research Centre. Therefore, model validation at a pilot plant or full scale level was not feasible. The research independence has resulted in certain freedom in the techniques employed and model assessments presented.

Model validation at the simulation model level was considered sufficient towards the achievement of the objectives of the research - the development of the SAG mill inferential models. This level of validation also leaves the simulation models in a state of readiness for further research and development.

3.6   Summary

In this Chapter, steady state models of the comminution circuit unit operations and the full circuit have been programmed into the MATLAB-Simulink environment and validated against industrial plant survey data, see Appendix B and Appendix C. Further supplementary validation was conducted against published data (Gault, 1975).

Generally, the models presented in this Chapter are those described in the Julius Kruttschnitt Mineral Research Centre Monograph (Napier-Munn *et al.*, 1996) and the JKSimMet User Manual (JKTech, 1994) and thus do not represent innovations of this research. One exception is the impact zone model developed independently in the course of this research, see Section 3.3.1, as indicated in Table 3.16, the Innovation Summary for this Chapter.

Table 3.16: Chapter 3 Innovation Summary

Section	Innovation
Section 3.3.1	SAG mill impact zone model